Lateral Control Of Front-wheel-steering Rubber-tire Vehicles

Article · January 1990

Source: RePEc

CITATIONS
71

READS
225

2 authors:

Huei Peng
University of Michigan
359 PUBLICATIONS **18,286** CITATIONS

SEE PROFILE

Masayoshi Tomizuka
University of California, Berkeley
1,030 PUBLICATIONS **25,689** CITATIONS

SEE PROFILE

Title:
Lateral Control Of Front-wheel-steering Rubber-tire Vehicles

Author:
Peng, Huei
Tomizuka, Masayoshi

Publication Date:
01-01-1990

Series:
Research Reports

Publication Info:
Research Reports, California Partners for Advanced Transit and Highways (PATH), Institute of Transportation Studies, UC Berkeley

Keywords:
Motor vehicles--Automatic control--Mathematical models, Motor vehicles--Dynamics--Mathematical models, Automobiles--Dynamics--Mathematical models

Abstract:
In this paper, two models were developed to describe the lateral dynamics of a vehicle for different purposes. The lateral feedback and feedforward controllers are designed to satisfy the above objective based on a linearized model, which includes only the lateral and yaw motions. The performance of the controllers is evaluated on a complex model, which includes motions in all six directions (longitudinal, lateral, vertical, roll, pitch and yaw). It has been validated by numerical simulations that the responses of the complex model and the simplified model remain close to each other when the steering is not too abrupt.

Program on Advanced Technology for the Highway
INSTITUTE OF TRANSPORTATION STUDIES
UNIVERSITY OF CALIFORNIA AT BERKELEY

Lateral Control of Front-Wheel-Steering Rubber-Tire Vehicles

Huei Peng
Masayoshi Tomizuka

UCB-ITS-PRR-90-5

July 1990

Abstract

The objectives of lateral control in the PATH project are to let vehicles track the center of a lane with small error and to maintain good ride quality under different vehicle speeds, loads, wind gust disturbances, and road conditions.

In this paper, two models were developed to describe the lateral dynamics of a vehicle for different purposes. The lateral feedback and feedforward controllers are designed to satisfy the above objective based on a linearized model, which includes only the lateral and yaw motions. The performance of the controllers is evaluated on a complex model, which includes motions in all six directions (longitudinal, lateral, vertical, roll, pitch and yaw). It has been validated by numerical simulations that the responses of the complex model and the simplified model remain close to each other when the steering is not too abrupt. The frequency-shaped linear quadratic (FSLQ) control theory is used for the design of the feedback controller. By using this design theory, the ride quality can be included in the performance index explicitly, and the high-frequency robustness characteristic can be improved by properly choosing the weighting factors. It is shown that a controller with fixed gains does not perform satisfactorily under all conditions. Therefore, an estimator for the cornering stiffness of tires is proposed to enhance performance. The gain-scheduling technique is used to tune the feedback and feedforward controllers utilizing the informations on C_s and V. Simulation results show that this adaptive control approach works satisfactorily under a variety of conditions including intermittent measurement of lateral tracking error.

1 Introduction

The lateral control of vehicles has been studied since late 1950' s[l]. Senders et al. [2] show that the lane keeping task needs little attendance from the driver, and is therefore regarded as an easy task to achieve [3][4]. The design of lateral controllers can be approached in two different ways. One is based on mimicing human driver behaviors [3],[5]-[7], and the other is based on vehicle dynamic models and control theories [8]-[l l]. The former approach does not require exact knowledge on the vehicle dynamics; it requires only a simple model representing the response characteristics of the vehicle (rise time, stability factor, damping,.. .) together with a controller simulating the "control algorithm" of a human driver. The latter approach usually requires a good dynamic model of the vehicle and then utilizes different control algorithms to achieve the specified goals(tracking, ride quality, etc). Two interesting issues of the lateral control problem remain relatively untouched. First, none of the previous works incorporate the ride quality explicitly though many researchers ([8],[9],[111) recognized its importance. Secondly, the system parameters (vehicle speed, load, and road condition) vary over a wide range, which makes it difficult to tune a fixed-gain controller. In this paper, the controller is designed based on the minimization of a performance index which includes both the tracking error and the ride quality. Furthermore, it is proposed to estimate time-varying vehicle parameters and to introduce adaptation capability to the controller so that its performance is acceptable over the entire operating range. For measurement of lateral tracking error, the discrete magnetic marker scheme[l2] is emphasized.

Two models are utilized to represent the lateral dynamics of a front-wheel-steering rubber-tire vehicle in this research: a complex model and a simplified model. The complex model, which includes the dynamics of the mass center of the vehicle in the three translational and three rotational directions, is a nonlinear model; and the simplified model, which includes only the lateral and yaw motions, is a linear model. The controllers are designed based on the simplified model, and their performance is evaluated on the complex model.

The overall controller consists of a feedback controller and a feedforward controller. The frequency-shaped linear quadratic (FSLQ) control theory is used for the design of the feedback controller. By using this design theory, the ride quality can be included in the performance index explicitly and, meanwhile, the high-frequency robustness characteristic can be improved by properly choosing the weighting factors of the performance index. If the curvature of the upcoming road is available as preview information, the performance of the controller could be further improved. The feedforward controller can generate the steady-state or

preview steering command corresponding to the curvature of the road.

The lateral dynamics of the vehicle strongly depends on the cornering stiffness C, and longitudinal velocity V. Their values change over a wide range. While V is normally measured, direct measurement of C_s is not easy to achieve. Furthermore, it is a state-dependent as well as input-dependent parameter. A parameter identification scheme is proposed to estimate the cornering stiffness from the measurement of lateral acceleration and yaw rate signals. The gain-scheduling technique is used to tune the feedback and feedforward controllers utilizing the informations on C_s and V.

The remaining content of this paper is organized as follows. The complex and simplified models are described in section 2. Open-loop simulation results of the two models are shown in section 3. Section 4 presents the design and analysis of controller and parameter identifier. Simulation results of this control system under various operating conditions are shown in section 5. Conclusions are given in section 6.

2 Modeling

Two models have been developed for the PATH project. A six-degree-of-freedom (DOF) nonlinear model is developed to represent the vehicle as realistically as possible. A simplified model is obtained by linearizing the complex model, and retains the lateral and yaw motion dynamics. The feedback and feedforward controllers are designed based on the simplified model and the performance evaluations are based on the numerical simulations on the complex model. Both models can describe four-wheel-steering, four-wheel-drive vehicles. However, in this paper they are used for front-wheel-steering, front-wheel-drive vehicles only, These two models are introduced in the following subsections.

Complex Model

The complex model describes the six DOF motions (three translational and three rotational) of the mass center of the vehicle. It is based on the model developed by Lugner[l3], and a tire model by Sakai[141 is introduced in place of the one used in [13]. The schematic diagram and the equations of the complex vehicle model are given in Appendix 1. The number of state variables is sixteen; twelve for the six DOF motions and four for the tires.

For the purpose of linearization, the following relation is used to define the effective value of the cornering stiffness C_s to be used in the simplified model:

$$C_s \equiv \frac{F_y}{\alpha} \tag{1}$$

where F_y is the lateral force generated from the tire, and a is the tire slip angle [14]. It should be noted that the cornering stiffness C,, which dominates the lateral dynamics of the vehicle, is not constant.

Simplified Model

The simplified model includes only the lateral and the yaw motions of the mass center of the vehicle. This model is obtained from the complex model. The equations and the schematic diagram of the simplified model are presented in Appendix 2.

In state space, the system can be expressed as:

$$\frac{d}{dt}\begin{bmatrix} y_r \\ \dot{y}_r \\ \varepsilon-\varepsilon_d \\ \dot{\varepsilon}-\dot{\varepsilon}_d \end{bmatrix} = \begin{bmatrix} 0 & 1 & 0 & 0 \\ 0 & \frac{A_1}{V} & -A_1 & \frac{A_2}{V} \\ 0 & 0 & 0 & 1 \\ 0 & \frac{A_3}{V} & -A_3 & \frac{A_4}{V} \end{bmatrix} \begin{bmatrix} y_r \\ \dot{y}_r \\ \varepsilon-\varepsilon_d \\ \dot{\varepsilon}-\dot{\varepsilon}_d \end{bmatrix} + \begin{bmatrix} 0 \\ B_1 \\ 0 \\ B_2 \end{bmatrix} \delta + \begin{bmatrix} 0 \\ d_1 \\ 0 \\ d_2 \end{bmatrix} = A\,\underline{x} + \underline{B}\,\delta + \underline{d} \tag{2}$$

where the variables and symbols are as defined in Appendix 2. Measurement of the lateral position of the vehicle is relative to the centerline of the roadway. If the measurement of lateral deviation from a sensor located at a distance d_s ahead of the mass center is chosen to be the output, it can be expressed as:

$$y_s = y_r + d_s\,(\,\varepsilon - \varepsilon_d\,) = [\,1,\,0,\,d_s,\,0\,]\,\underline{x} \tag{3}$$

This measurement would be available continuously from a guidance wire reference or intermittently from a discrete marker reference [12]. In this paper, the latter reference scheme is emphasized. The transfer function from the front wheel steering angle $\delta(s)$ to the output y,(s) is:

$$\frac{y_s(s)}{\delta(s)} = \frac{1}{\Delta(s)}\left[(d_sB_2+B_1)s^2 + \frac{d_s(B_1A_3-B_2A_1)+B_2A_2-B_1A_4}{V}s + B_1A_3-B_2A_1\right] \tag{4}$$

where

$$\Delta(s) = s^2\left[s^2 - \frac{A_1+A_4}{V}\,s + \frac{(A_1A_4-A_2A_3)}{V^2} + A_3\right] \tag{5}$$

The vehicle dynamics depends on the cornering stiffness (C_s), which dominates the characteristics of the tire-road interaction, the load (m, I_z), and longitudinal velocity (V). The value of C_s is affected by many factors. In addition to the tire slip ratio and the tire slip angle as explained in Appendix 1, it depends on the tire pressure, load, velocity, temperature, and most of all, the road conditions [15][161. The nominal and extreme values of these parameters are summarized in Table 1. Figures l-3 are the Bode plots of the transfer functions of the vehicle model (4) when one of the three system parameters (V, C_s, and $m(I_z)$) changes. It is clear that the cornering stiffness C_s and the velocity V are the dominant parameters. They vary in a wide range and change the response of the system drastically.

Table 1 System parameters of the simplified model

parameter	symbol	nominal value	min	max
mass (kg)	m	1550	0.85(*)	1.15(*)
moment of inertia ($kg-m^2$)	I_z	3100	0.85(*)	1.15(*)
cornering stiffness (N/rad)	C_s	42000	0.2(*)	2.0(*)
longitudinal velocity (mi/hr)	V	70	25	85
base length (m)	l_1 l_2	1.15 1.51	-	-
magnetic sensor position (m)	d_s	1		

(*) relative to the nominal value

3 Open-loop Simulations

The objective of the open loop simulations is to confirm that the responses of the complex and the simplified models remain close to each other under typical operating conditions.

The system parameters of the complex and simplified models used in the open-loop simulations are given in Table A.1 and Table 1 respectively. Three types of input signals are used in the simulations: sinusoidal, ramp, and trapezoidal. For the steering commands shown in Figure 4, the simulated responses by the complex and the simplified model are as shown in Figure 5. Responses of the complex model and those of the simplified model remain close to each other, i.e., the simplified model is a good approximation of the complex model for typical inputs. However, the final justification will be based on the closed-loop simulation with the complex model.

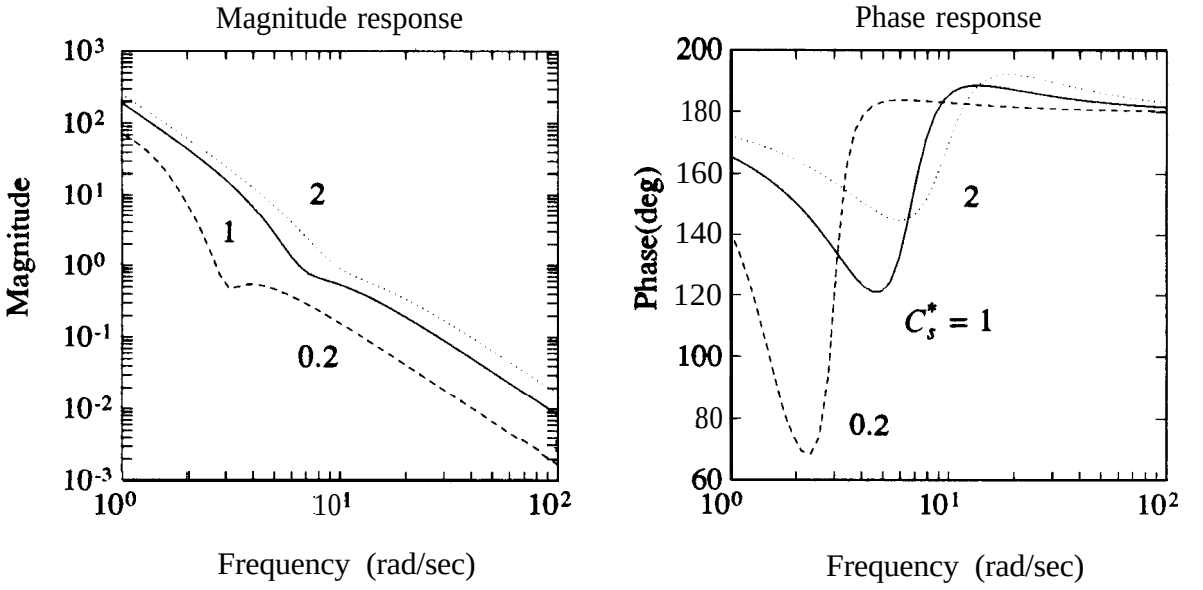

Figure 1 Bode plot of vehicle transfer function model
Variations due to C_s

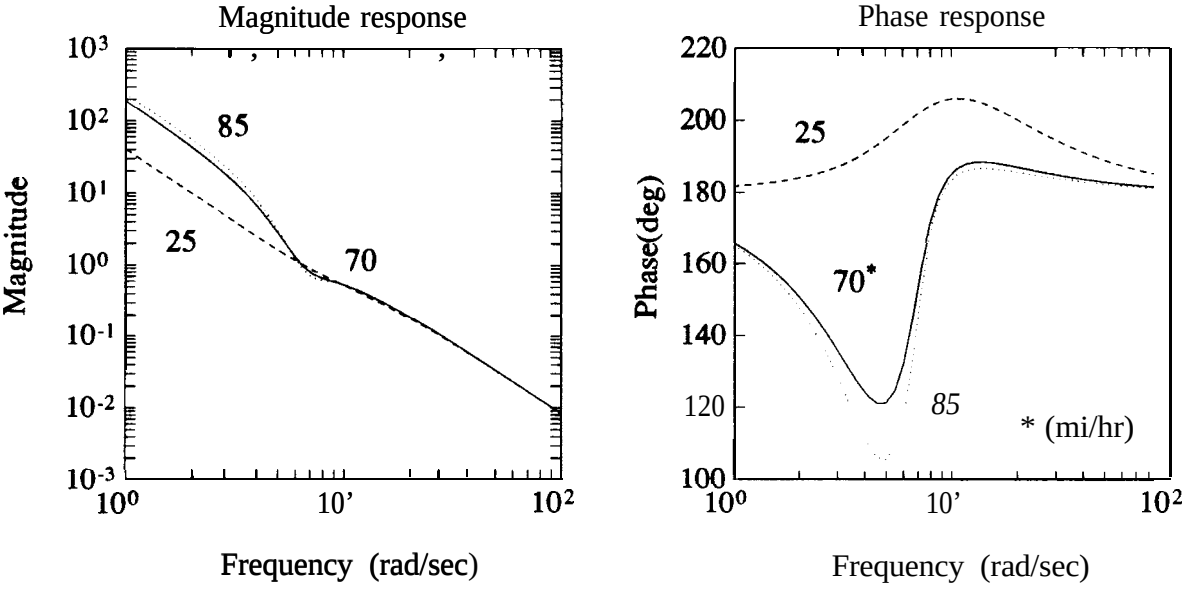

Figure 2 Bode plot of vehicle transfer function model
Variations due to *V*

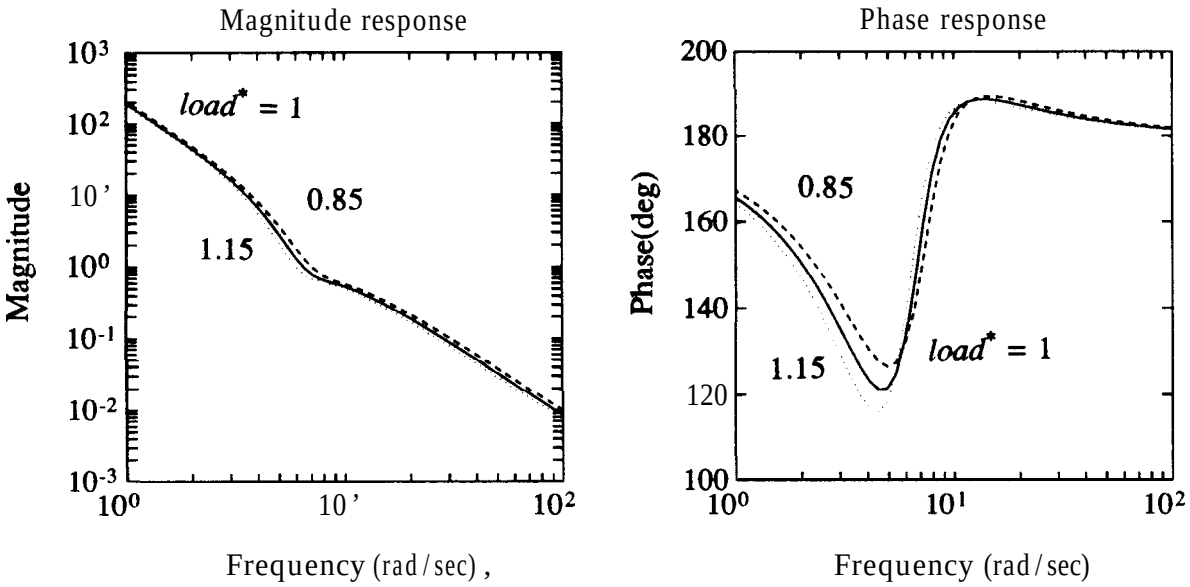

Figure 3 Bode plot of vehicle transfer function model
Variations due to m, I_z

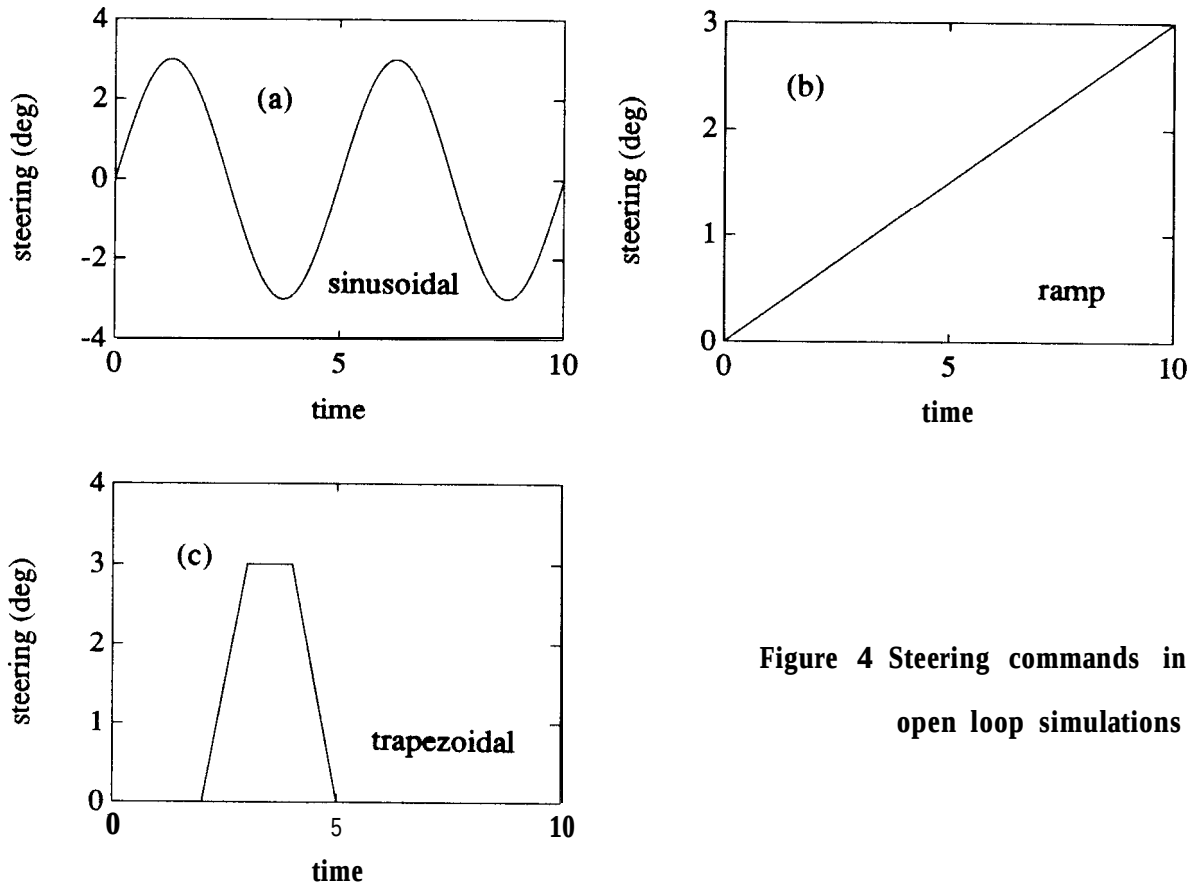

Figure 4 Steering commands in open loop simulations

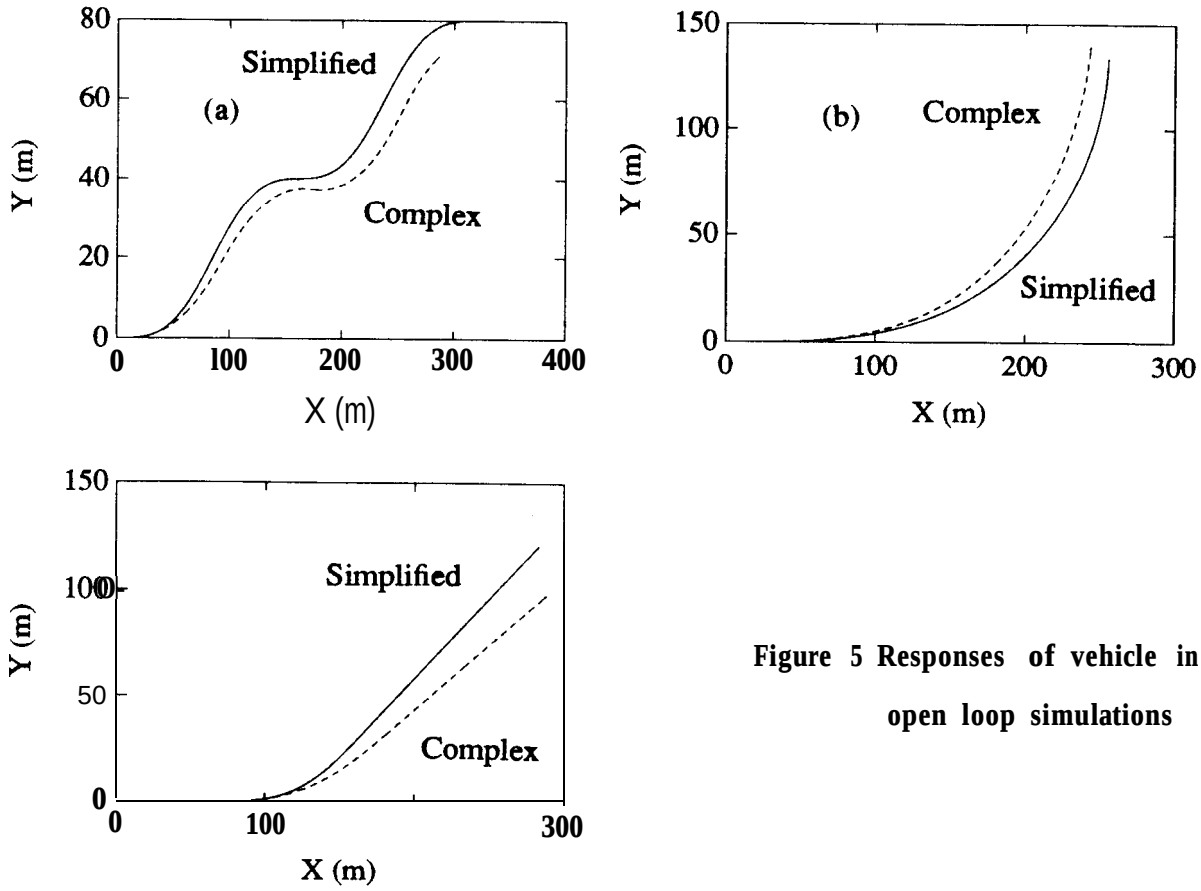

Figure 5 Responses of vehicle in open loop simulations

4 Controller Design

As pointed out before, the control objective is to keep the tracking error small while maintaining good ride quality under widely varying system parameters. High gain robust controllers deteriorate ride quality and are not considered to be serious candidates. The overall controller in this paper consists of a feedback part and a feedforward part. The gains of the controllers are tuned based on the values of the system parameters C_s, V, m, and I_z. While V, m and I_z can be easily measured or estimated, the estimation of C_s is not straightforward. The frequency-shaped linear quadratic (FSLQ) control theory is used to design the feedback controller. Assuming that the radius of curvature of the current road is available, the steady-state steering signal command is generated by the feedforward controller to improve the system response. Notice that both the feedback and feedforward controllers are dependent on the estimation of the cornering stiffness.

4.1 FSLQ Controller

The FSLQ control theory [17][18] provides a controller design tool for a linear system based on the minimization of a quadratic performance index, which includes the frequency as a parameter. The FSLQ control theory has the following advantages in the design of the lateral control problem.

(1) Frequency dependent weighting factors are placed on the tracking error, lateral acceleration, and control effort terms in the performance index to compromise these conflicting objectives.

(2) The weighting factors on the tracking error terms can be shaped in the frequency domain to enhance the robustness of the controller when the plant is subject to high frequency measurement noises or unmodeled dynamics. Meanwhile, the tracking ability in the low frequency region is not deteriorated.

(3) The weighting factor on the lateral acceleration term can be shaped in the frequency domain so that a good ride quality is assured in the frequency range where passengers are sensitive.

The formulation of the performance index and shaping of individual weighting factors to realize these advantages are presented below.

Formulation of the Performance Index

The feedback controller is designed by minimizing the performance index:

$$J = \frac{1}{2\pi}\int_{-\infty}^{\infty}[a^*(j\omega)Q_a(j\omega)a(j\omega) + y_r^*(j\omega)Q_y(j\omega)y_r(j\omega) \tag{6}$$
$$+ (\varepsilon(j\omega)-\varepsilon_d(j\omega))^*Q_\varepsilon(j\omega)(\varepsilon(j\omega)-\varepsilon_d(j\omega)) + y_s^*(j\omega)Q_i(j\omega)y_s(j\omega) + \delta^*(j\omega)\delta(j\omega)]d\omega$$
$$= \frac{1}{2\pi}\int_{-\infty}^{\infty}[a^*(j\omega)\frac{q_a^2}{1+\lambda_a^2\omega^2}a(j\omega) + y_r^*(j\omega)\frac{q_y^2}{1+\lambda_y^2\omega^2}y_r(j\omega)$$
$$+ (\varepsilon(j\omega)-\varepsilon_d(j\omega))^*\frac{q_\varepsilon^2}{1+\lambda_\varepsilon^2\omega^2}(\varepsilon(j\omega)-\varepsilon_d(j\omega)) + y_s^*(j\omega)\frac{q_i^2}{(j\omega)^2}y_s(j\omega)+\delta^*(j\omega)\delta(j\omega)]d\omega$$

In Eq.(6) a is the difference between the lateral acceleration $\ddot{y}_a$ and its desired value, and is expressed as:

$$a = \ddot{y}_a - \frac{V^2}{\rho} \approx \ddot{y}_r \tag{7}$$

where ρ is the radius of curvature of the road, and y_r is the lateral deviation of the mass center from the reference (magnetic markers).

The coefficient λ_a determines the weighting on each frequency component in the lateral acceleration, and is crucial for ride quality. Coefficients λ_y and λ_ε are tuned to enhance the high-frequency robustness of the controller while maintaining good tracking capability. After choosing the values of λ_a, λ_y and A,,, the values of q_a, q_y, q_ε and q_i are adjusted for further tuning.

Ride Qualitv

The ride quality is reflected in the lateral acceleration term of the performance index. Many standards have been developed to express the ride quality in terms of a frequency-dependent weighting index on the lateral acceleration. Among them are the ISO[19], and *rms*[20] specifications. It has been shown [21] that all these specifications can adequately describe the ride quality. In order not to increase the number of augmented state variables excessively, the weighting is simplified to the one shown in Figure 6. In particular, λ_a is set to be $\frac{1}{60\pi}$.

High-freauencv Robustness

The relative degree of the simplified model is two. Therefore, the gain of the transfer function decays with $-40dB/dec$ in the high-frequency range. In other words, high frequency components of the steering command do not excite the output y_s as much as low frequency components. High frequency components in the steering input are not desirable because of the following two reasons: they deteriorate the ride quality and they may excite unmodeled dynamics of the vehicle.

It is well-known that better robustness in the high-frequency range can be achieved by reducing the gain. Therefore, it is recommended to shape the weighting factors $Q_y(j\omega)$ and $Q_\varepsilon(j\omega)$ to the one shown in Figure 6. This results in a smaller control gain in the high frequency range, and improves the robustness of the system. The steady state tracking error approaches zero because of the integral action introduced by $Q_i(j\omega)$.

The coefficients λ_y and λ_ε are tuned to satisfy two performance requirements: tracking capability and measurement noise rejection capability. $\frac{1}{2\pi\lambda_y}$ and $\frac{1}{2\pi\lambda_\varepsilon}$ should be larger than the maximum frequency of the desired reference signal to have good tracking performance. On the other hand, they should be smaller than the rate of measurements so that the high frequency measurement noises and alias noises are attenuated.

According to [22], the minimum designed radius of curvature ρ of the freeway is, roughly speaking, a function of the designed vehicle speed V_d. Assuming that the speed V of the vehicle is less than or equal to the designed speed V_d, *we* obtain

$$a_{lateral} = \frac{V^2}{\rho} \le \frac{V_d^2}{\rho} \le a_{\max} \tag{8}$$

where $a_{\max}$ is the maximum allowable lateral acceleration. To have good tracking capability, we should have:

$$\frac{1}{\lambda_y(V)}, \frac{1}{\lambda_\varepsilon(V)} \ge \max \mid \dot{\varepsilon}_d(V) \mid = \max \mid \frac{V}{\rho} \mid = \frac{a_{\max}}{V} \tag{9}$$

For the discrete marker reference scheme[23], to have good high frequency robustness, the following relation should be satisfied:

$$\frac{1}{2\pi\ \lambda_y(V)}, \frac{1}{2\pi\ \lambda_\varepsilon(V)} \le f_m(V) = \frac{V}{D_f} \tag{10}$$

where f,(V) is the rate of measurement in Hz and Df is the spacing between two adjacent markers in the discrete marker scheme.

From (9) and (lo), λ_y and λ_ε are chosen to be:

$$\lambda_y, \lambda_\varepsilon = \left(\frac{D_f}{2\pi a_{\max}}\right)^{\frac{1}{2}} \tag{11}$$

Transient and Steady-state Responses

After choosing λ_a, λ_y, and λ_ε, parameters q_a, q_y, q_ε and q_i are tuned to compromise the ride quality and the tracking error. The FSLQ problem can be transformed to a standard LQ problem by introducing augmented state variables, and the gain vector of the feedback controller can be computed by solving a Riccati equation. Details of the FSLQ design are given in Appendix 3.

It should be noted that in solving the FSLQ problem by transforming it to a LQ problem, the system order will be increased because of the introduction of augmented state variables. In our problem, the augmented system is of eighth order; therefore, when the system parameters V and C_s vary, it is impossible to match the responses arbitrarily close to those of the nominal system by tuning four parameters q_a, q_y, q_ε, and q_i. That is, the responses vary when the system parameters change.

4.2 Feedforward Controller

The freeways in California are designed to have fixed curvatures, and transient spiral curves are not standard [22]. Therefore, if the radius of a curved section is known, the steering angle can be set constant at curved sections, From the simplified model, if the radius of curvature p is given, the corresponding steady state steering angle δ can be computed from:

$$\delta = \frac{V^2 A_3 - A_2 A_3 + A_1 A_4}{\rho(A_3 B_1 - A_1 B_2)} \tag{12}$$

where A_i and B_i are system parameters defined in Appendix 2. The feedforward controller sets the steering command in accordance with Equation (12). A more sophisticated usage of curvature information is possible if it is given as preview information[24]. Work is in progress to incorporate preview informations in the FSLQ controller and will be discussed further in details in the next report. It should be noted that the effect of the superelevation has not been included in Eq.(12).

4.3 Estimation of the cornering stiffness C_s

As described in section 4.1, the FSLQ performance index and hence the feedback controller depend on the cornering stiffness C_s and the longitudinal velocity V. V may change quickly, but its value can be easily measured. C_s is usually slow-varying, but its value is difficult to obtain. Furthermore, C_s may change abruptly in some cases: e.g. hitting a patch of ice. An estimation scheme for C_s is described below.

Assuming that the estimation of the "average" C_s for the four wheels is good enough from the viewpoint of the gain scheduling, that is, $C_{s_i} = C_s\, i=1..4$, we obtain from the simplified model:

$$m\ddot{y}_a = m(\ddot{y}_r + \frac{V^2}{\rho}) = 2C_s[\delta - \frac{2\dot{y}}{V} + \frac{(l_2-l_1)\dot{\varepsilon}}{V}] \qquad (13)$$

where $\ddot{y}_a$ is the lateral acceleration of the mass center. If $\ddot{y}_a$ and $\dot{\varepsilon}$ are measured by a lateral accelerometer and a yaw-rate sensor, and $\dot{y}$ is computed from $\ddot{y}_a$, then C_s can be estimated based on Eq.(13). The least squares algorithm with a forgetting factor [25] has the following form:

$$\hat{C}_s(k) = \frac{Num(k)}{Den(k)} = \frac{\kappa\, Num(k-1) + a_m(k)b_m(k)}{\kappa\, Den(k-1) + b_m^2(k)} \qquad (14)$$

where $Num(0)$ and $Den(O)$ must be assigned, and

$$a,(i) = m\ddot{y}_a(i) \qquad (15)$$

$$b,(i) = 2[\delta(i) - \frac{2\dot{y}(i)}{V(i)} + \frac{(l_2-l_1)\dot{\varepsilon}(i)}{V(i)}] \qquad (16)$$

The forgetting factor κ is set to be less than one to prevent the adaptation ability from dying away as time increases. Figure 7 shows the result of a simulation with the complex model when the vehicle is driven on a curved section as shown in Figure 8. The vehicle is controlled by the FSLQ feedback and feedforward controller with nominal system parameters listed in Table 1. It should be noted that the estimation scheme is turned off when the steering angle is small. This is for avoiding the parameter drift when the excitation signal is not suited for parameter identification. If the signal magnitude drops down below a certain value, it is difficult to conclude whether the error is due to parameter mismatches or noises. The estimation algorithm identifies the change of C_s with small time lag (< 0.2 set). However, the estimation can be adversely affected by wind gust and measurement noises. Also, when the vehicle is driving on a straight road section, there is a noticeable error (7%). The estimation algorithm in Eq.(14) relies on the measurements $\ddot{y}_a$ and $\dot{\varepsilon}$. Care must be taken on the measurement of

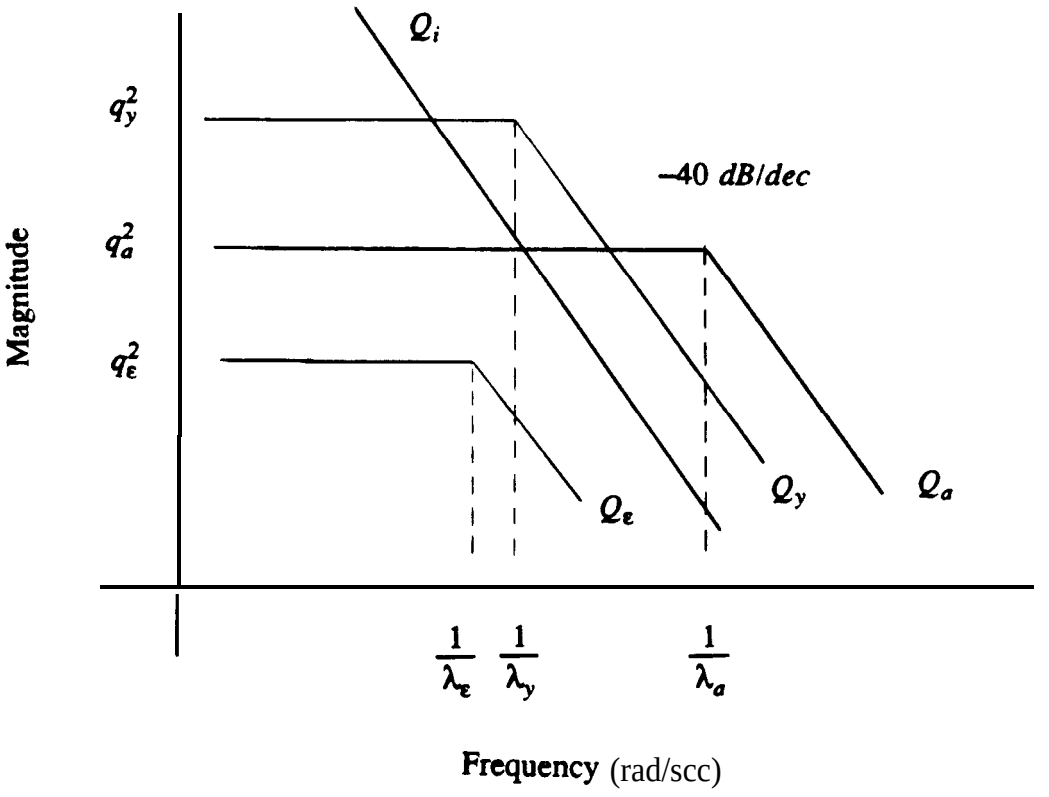

Figure 6 Weighting factor $Q_a(j\omega), Q_y(j\omega), Q_\varepsilon(j\omega)$ and $Q_i(j\omega)$

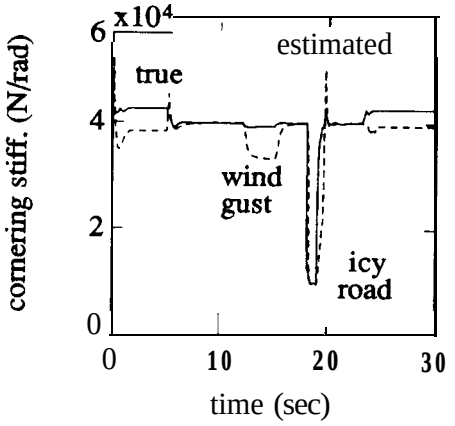

Figure 7 Estimation result of parameter identifier

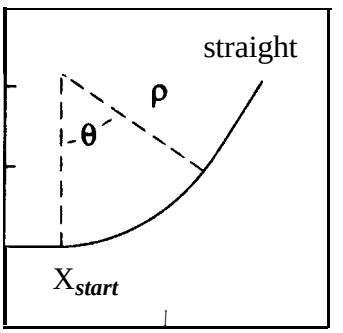

Figure 8 Geometry of desired trajectory

$\ddot{y}_a$ on a superelevated section because of the gravity component.

The simplified model (2) ignores the steering actuator dynamics. In the simulation study presented in the next section, the actuator dynamics were assumed to be :

$$\frac{\delta}{\delta_d} = \frac{1}{1+\tau s} \tag{17}$$

where δ_d is the steering command from the controller, δ is the actual steering angle from the actuator, and τ is the first order time constant of the actuator. The structure of the overall vehicle lateral control system is shown in Figure 9, where G_i and z_i represent the augmented dynamics and state variables respectively. See Appendix 3 for details.

5 Numerical Simulations

In the simulations, it is assumed that the values of p, V, m and I_z are available, and the gain scheduling technique is used to tune the gains of controllers automatically. The gains are pre-computed based on the FSLQ theory as functions of C_s and V. The measurement rates are assumed to be 100 Hz unless otherwise stated. Simulations with the vehicle speeds 10, 32 and $40m/sec$ are presented for comparison. The first order time constant of the actuator τ is assumed to be 32 msec. The controller is evaluated on the desired trajectory shown in Figure 8. The curve parameters are summarized in Table 2. Initial conditions in the simulations were $y_r = 20cm$ and $\varepsilon - \varepsilon_d = 0^o$. It should be emphasized again that all the simulations are performed on the complex model.

Table 2 Parameters of the desired trajectories

velocity (m/sec)	X_{start} (m)	ρ (m)	θ (deg)	time (set)
10	50	50	206.265	30
32	160	630	52.385	30
40	200	1500	27.502	30

Nominal case

Figure 10 shows the simulation results of the nominal system without any disturbances and measurement noises. The overshoot due to the initial position error of 20 cm is less than 10% and the overshoot due to the curved section is less than 6cm. The maximum lateral acceleration is kept small (O.lg) except in the curved section.

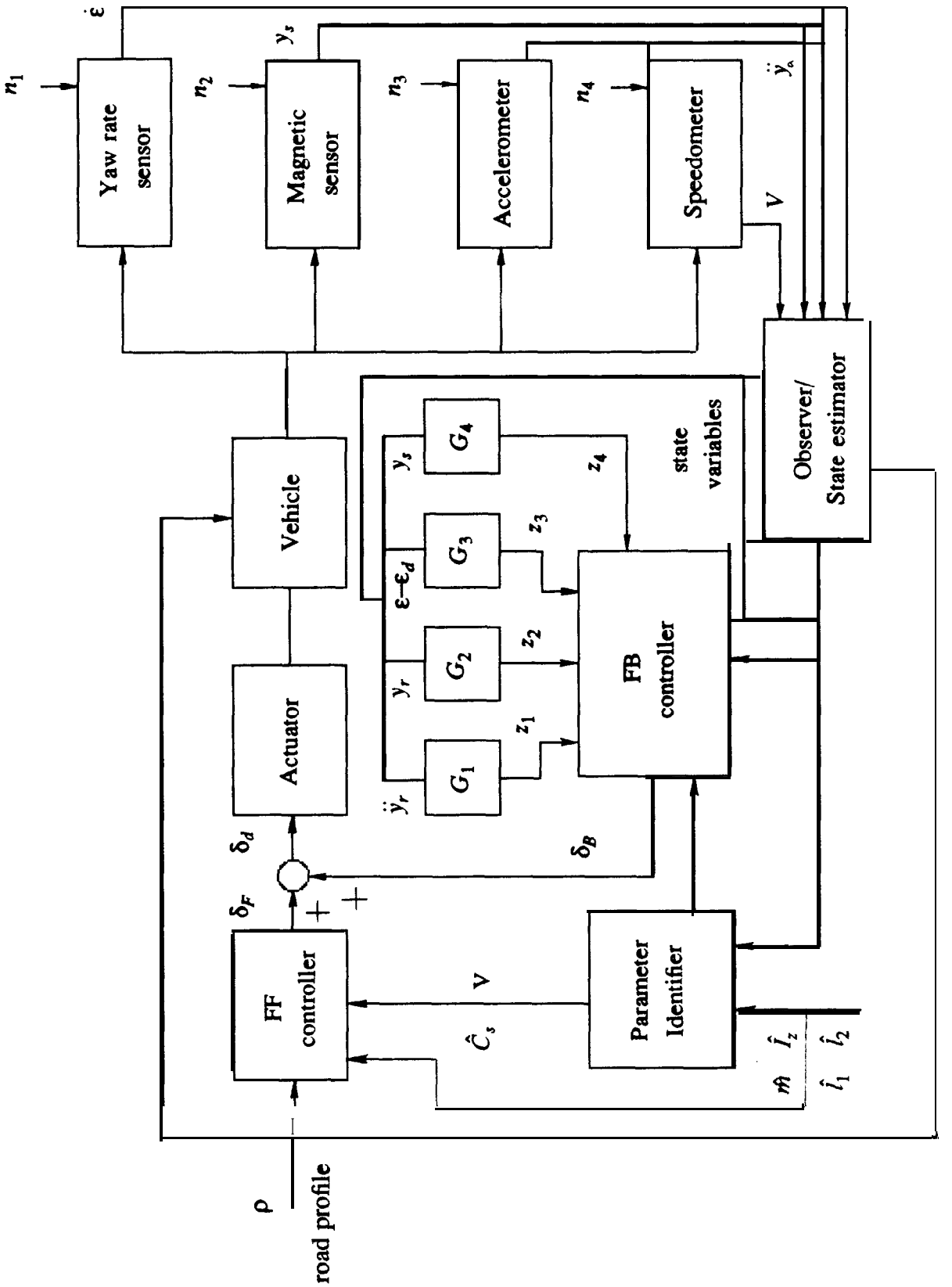

Figure 9 Schematic diagram of the overall system

Wind gust disturbance

Figure 11 shows the results when the vehicle is subject to wind gust with net force of -500 Newtons and moment of -200 Newton-meters in the lateral direction for three seconds. It can be seen that the controller quickly responds to the wind. Both the lateral deviation and acceleration are not significantly affected by the disturbances. Also, it can be seen that the effect of the wind gust increases when the velocity of the vehicle increases.

Discrete marker scheme

Figure 12(a) shows the results when the discrete markers are placed at a spacing of 10 feet, which determines the measurement rate of the lateral position deviation. All other measurements are performed at the rate of 100 Hz. The overshoot due to the initial position error is larger than those of the nominal cases. When the vehicle speed decreases, the deterioration becomes more significant. The steering and acceleration signals are more abrupt, especially when the vehicle speed is low and the curvature of the road changes. Figure 12(b) shows the responses of the vehicle with different marker spacing. The vehicle speed is l0m/sec and the lateral deviation measurement is assumed to be contaminated by the noise listed in Table 3. It can be seen that the lateral tracking error becomes more oscillatory when the spacing increases. Simulation results show that at the speed of 10m/sec, the maximum allowable spacing between markers is around 17 feet. However, when the vehicle speed increases, this allowable spacing will also increase.

ICY road

The road conditions are assumed to be unchanged in all of the above simulations. In this simulation, it is assumed that a section of the road is icy and causes the value of C_s drop to its minimum value for one second in the curved section. It can be seen from Figure 13 that the tracking error is kept to be less than 20 cm, which is the working range of the magnetic markers investigated in the PATH project [23]. A controller with fixed gain corresponding to the nominal system (V = 32*mlsec)* has a maximum tracking error of 26 *cm,* and is considered as unacceptable. This calls for the necessity of gain scheduling. It should be noted that the time delay between the front wheels and rear wheels is considered. It was found in the simulations that if this effect is not considered, the maximum lateral deviation will be 30-40% less because the yaw rotation due to this time delay is not considered.

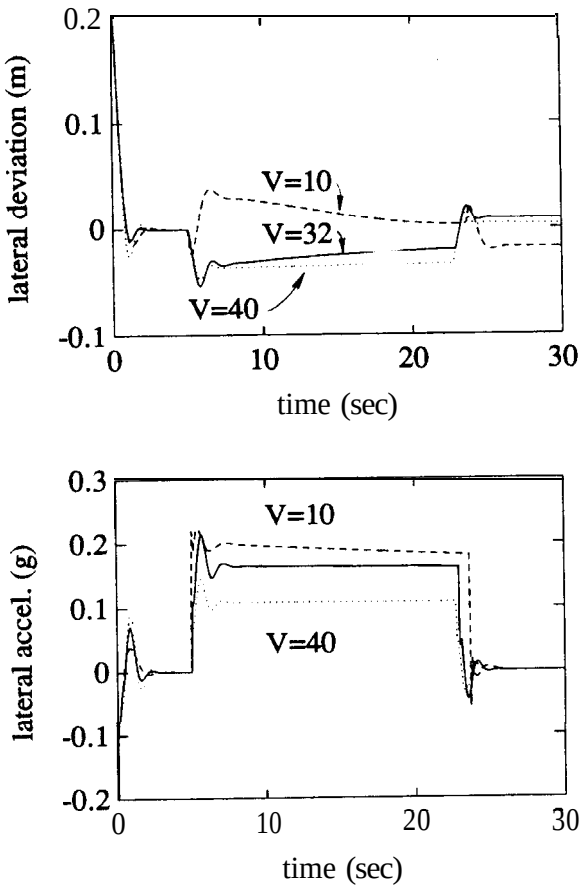

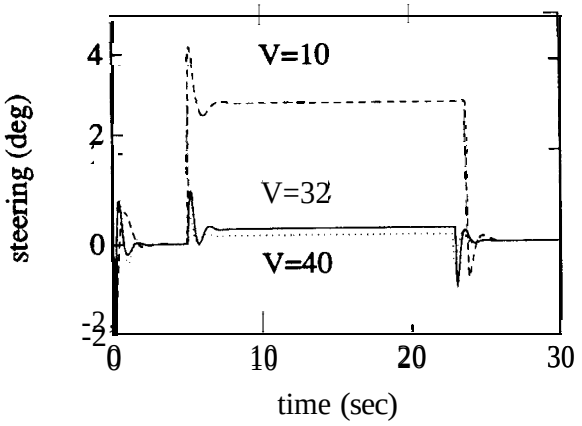

Figure 10 Simulation result of nominal case

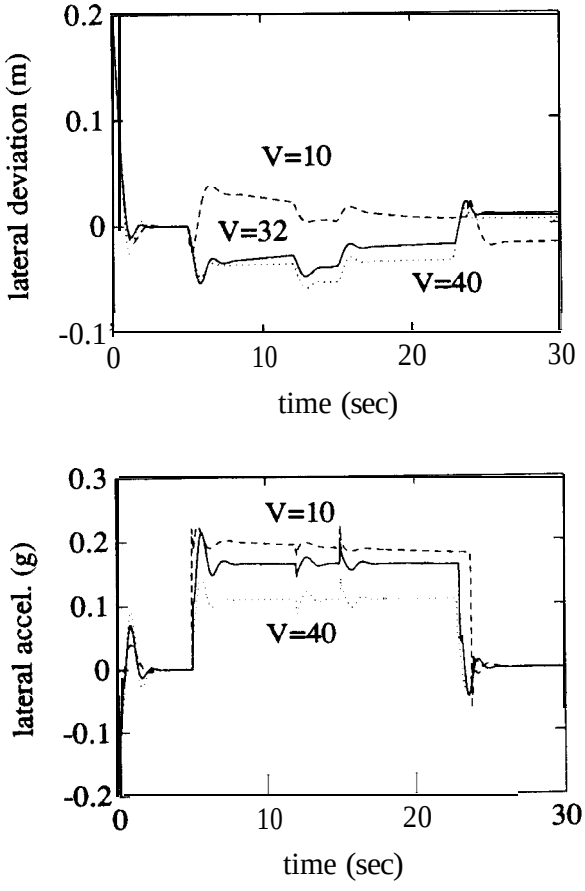

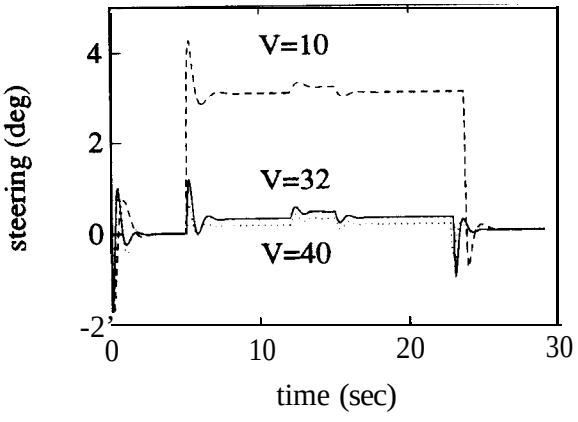

Figure 11 Simulation result with wind gust

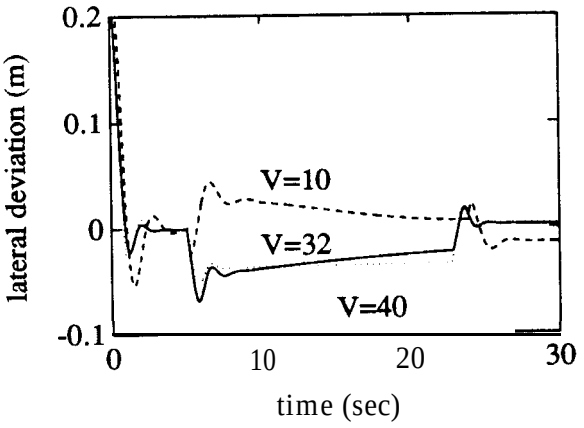

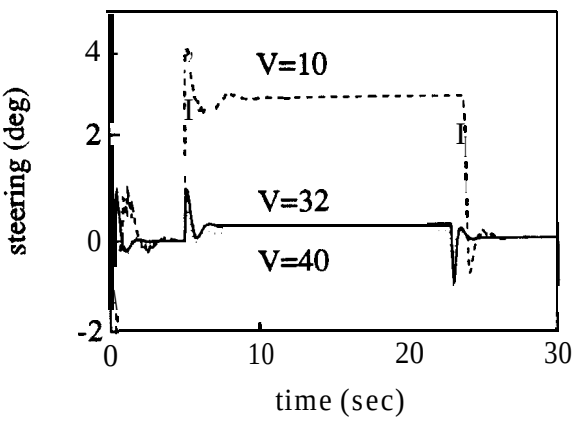

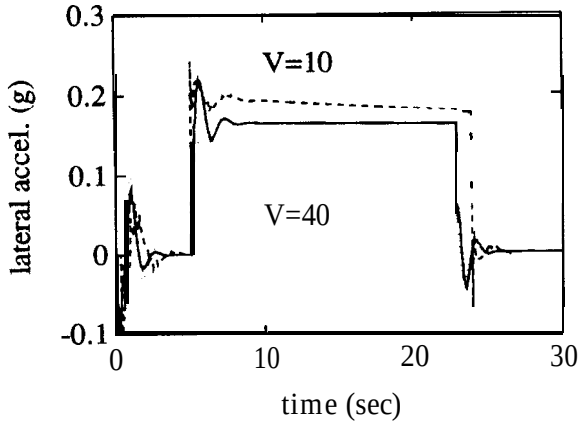

Figure 12(a) Simulation result with discrete marker scheme

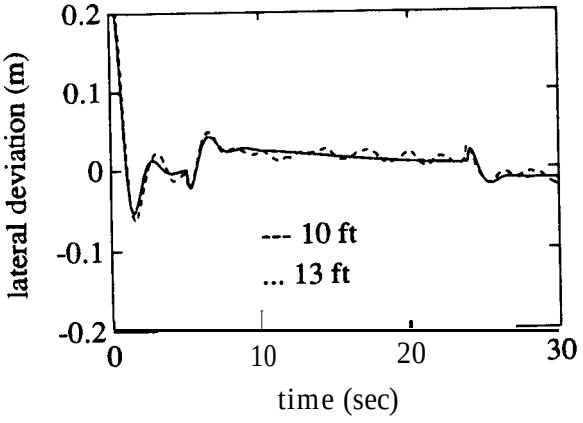

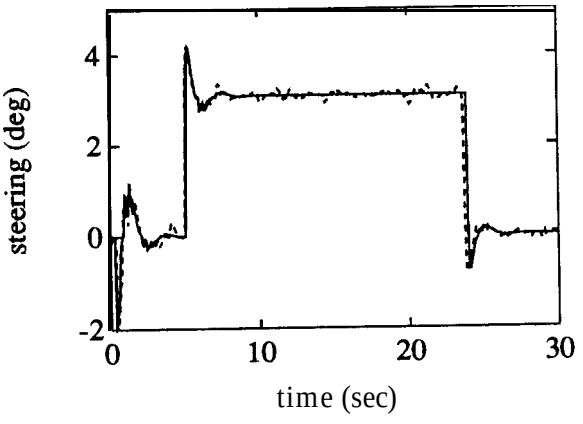

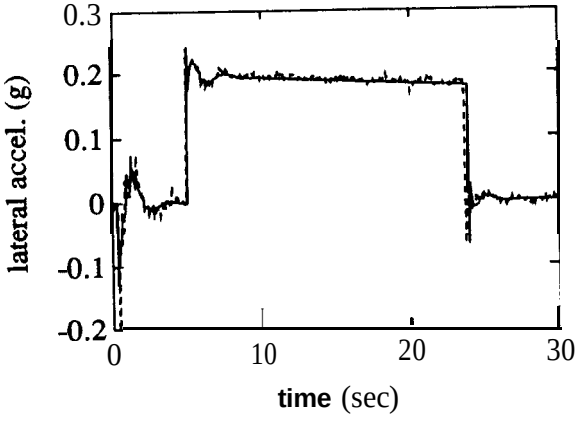

Figure 12(b) Simulation result with discrete marker scheme and measurement noises

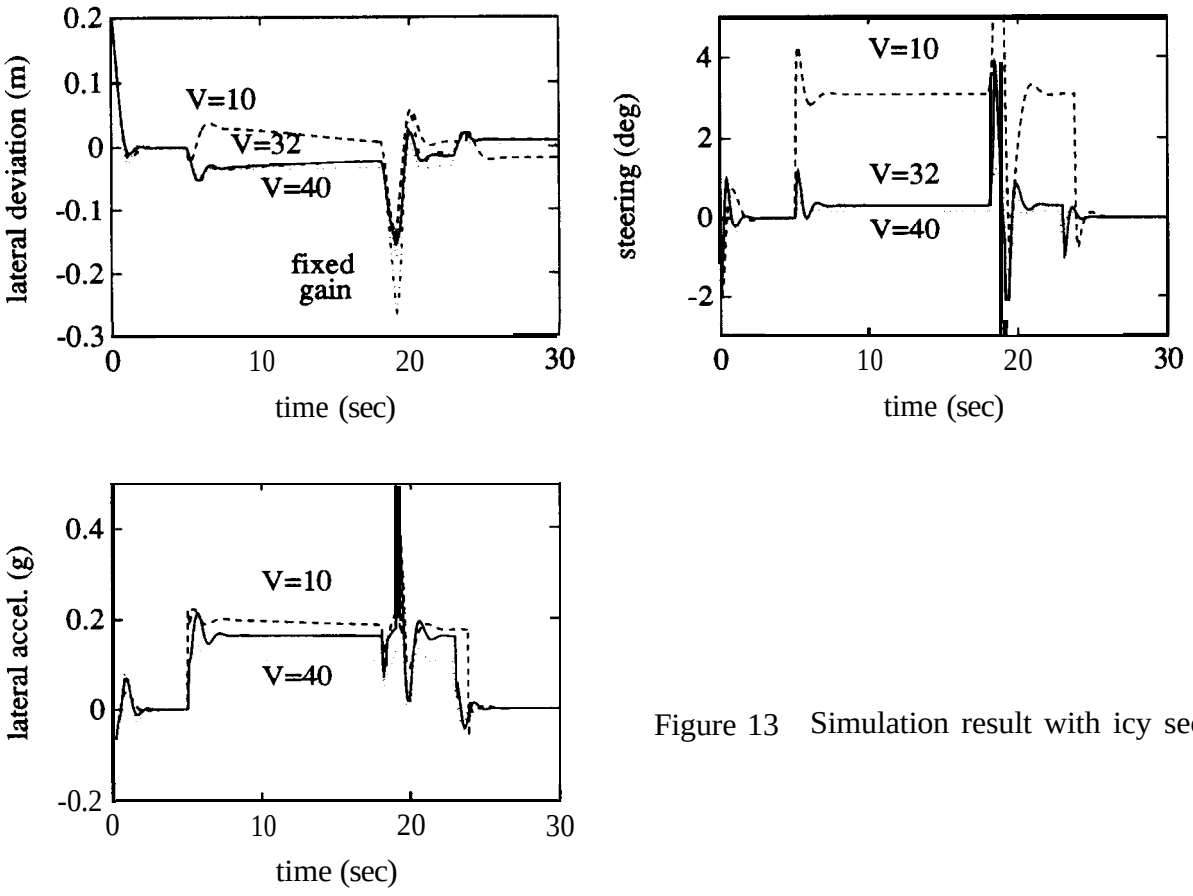

Figure 13 Simulation result with icy section

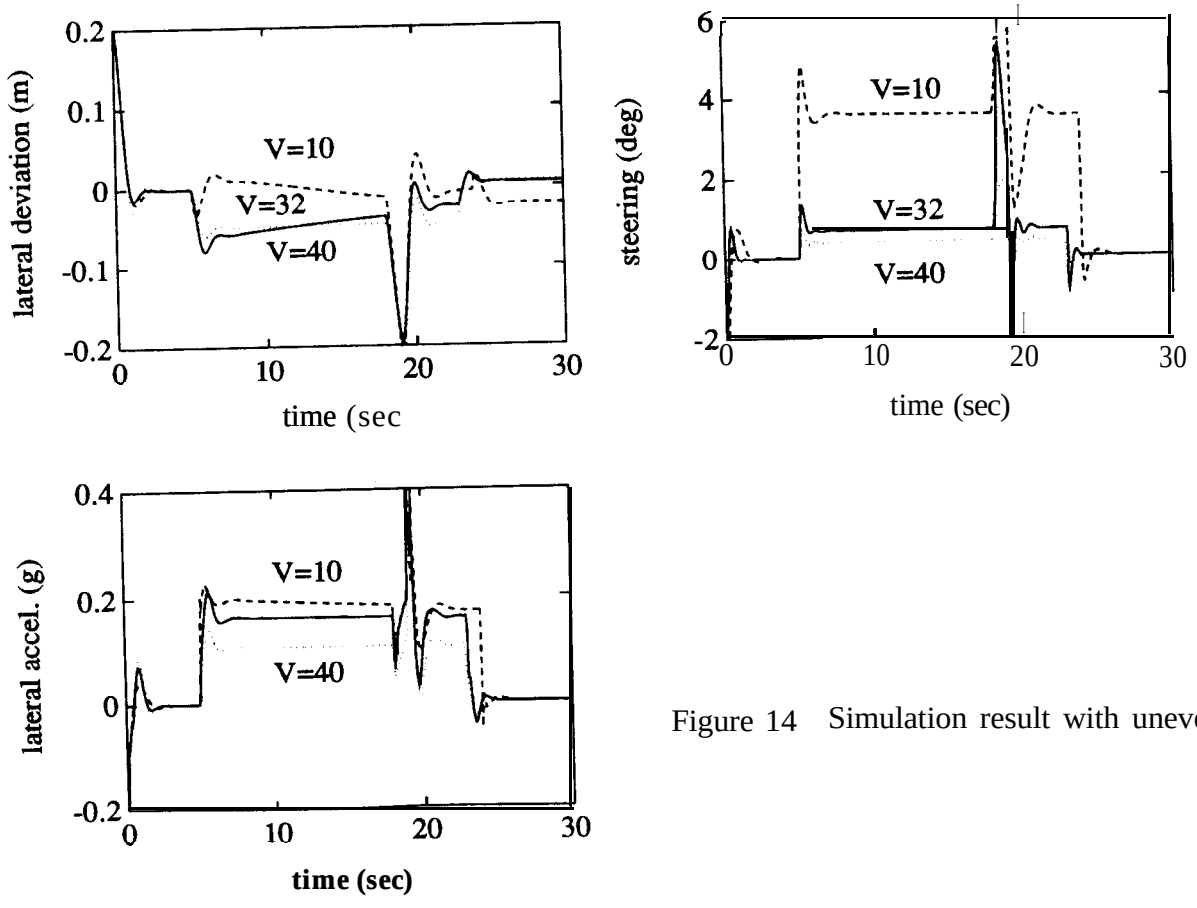

Figure 14 Simulation result with uneven C_s

Uneven tire cornering stiffness

As pointed out earlier in section 3, many factors affect the cornering stiffness C_s of a tire. Assuming that for some reasons, the cornering stiffness C_s is not uniform among the four tires. Figure 14 shows the case when the C_s of the rear tires are 50% higher than those of the front tires and the (one second) icy section is also present. It can be seen that the performance is still acceptable although the overshoots in the icy section become larger. This suggests that the estimation of the average cornering stiffness is good enough for the gain scheduling purposes.

Combined effects

Figure 15 shows the result when the wind gust, discrete marker scheme (with spacing of 10 ft) and icy road are all present. Furthermore, the measurements are assumed to be contaminated by the noises listed in Table 3. The performance is acceptable except that when V=10m/sec, the overshoot in acceleration is too high (0.43g) when the vehicle enters the icy section.

Table 3 Measurement noises

measurements	symbol	type	magnitude(*)
mass (kg)	m	offset	5
moment of inertia ($kg-m^2$)	I_z	offset	10
lateral position (m)	y_r	Gaussian	0.005
yaw rate ***(radlsec)***	ε	Gaussian	0.005
lateral accel (g)	$\ddot{y}_a$	Gaussian	***0.0005***
longitudinal Velocity (m/sec)	V	Gaussian	0.05
base length (m)	l_1 l_2	offset	0.04

(*) magnitude of offset/standard deviation of Gaussian white noise

Braking

The controller should perform satisfactorily not only under normal driving conditions, but also under emergency conditions. Figure 16 presents the responses of the vehicle when the vehicle is decelerating at the rate of -0.5g. The initial vehicle speed is 32 m/sec and the initial tracking error is 5 cm. Furthermore, the braking forces from the front wheels are assumed to be 80% larger than

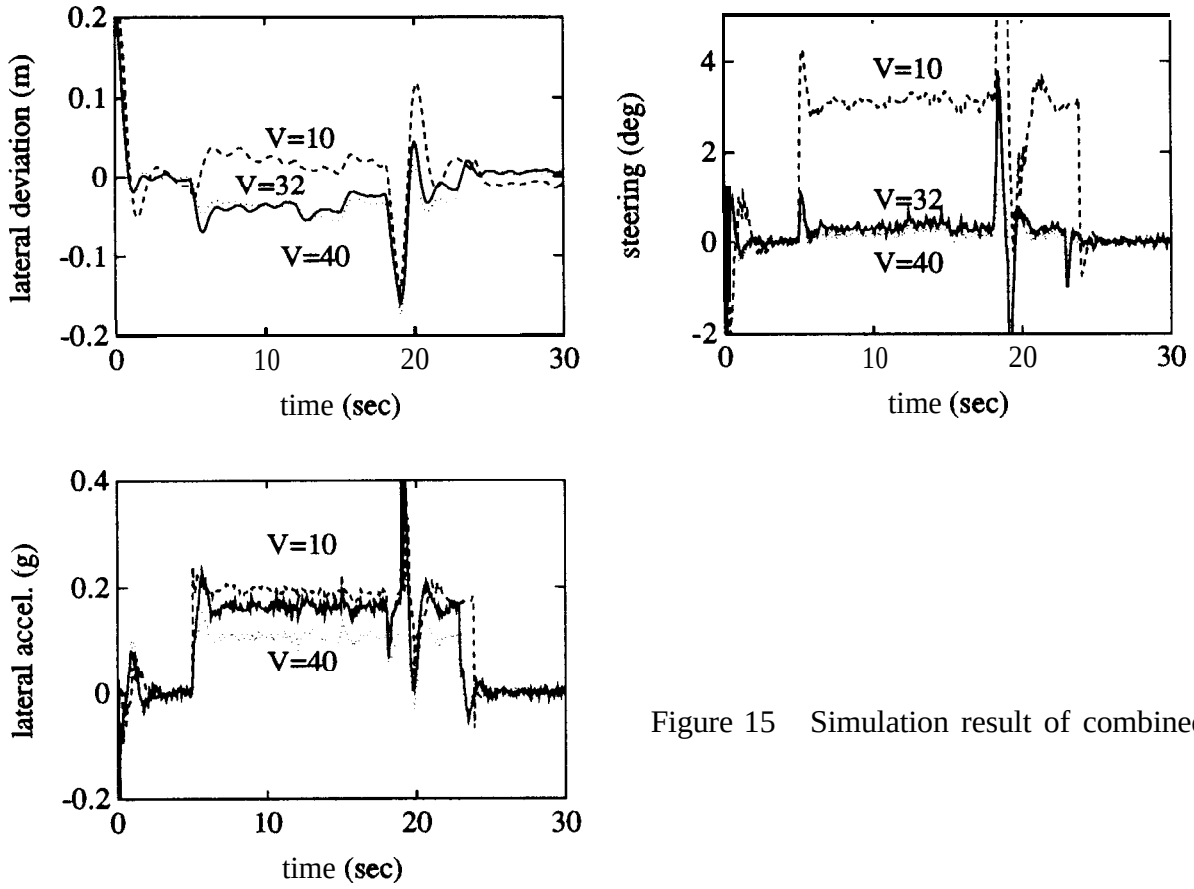

Figure 15 Simulation result of combined case

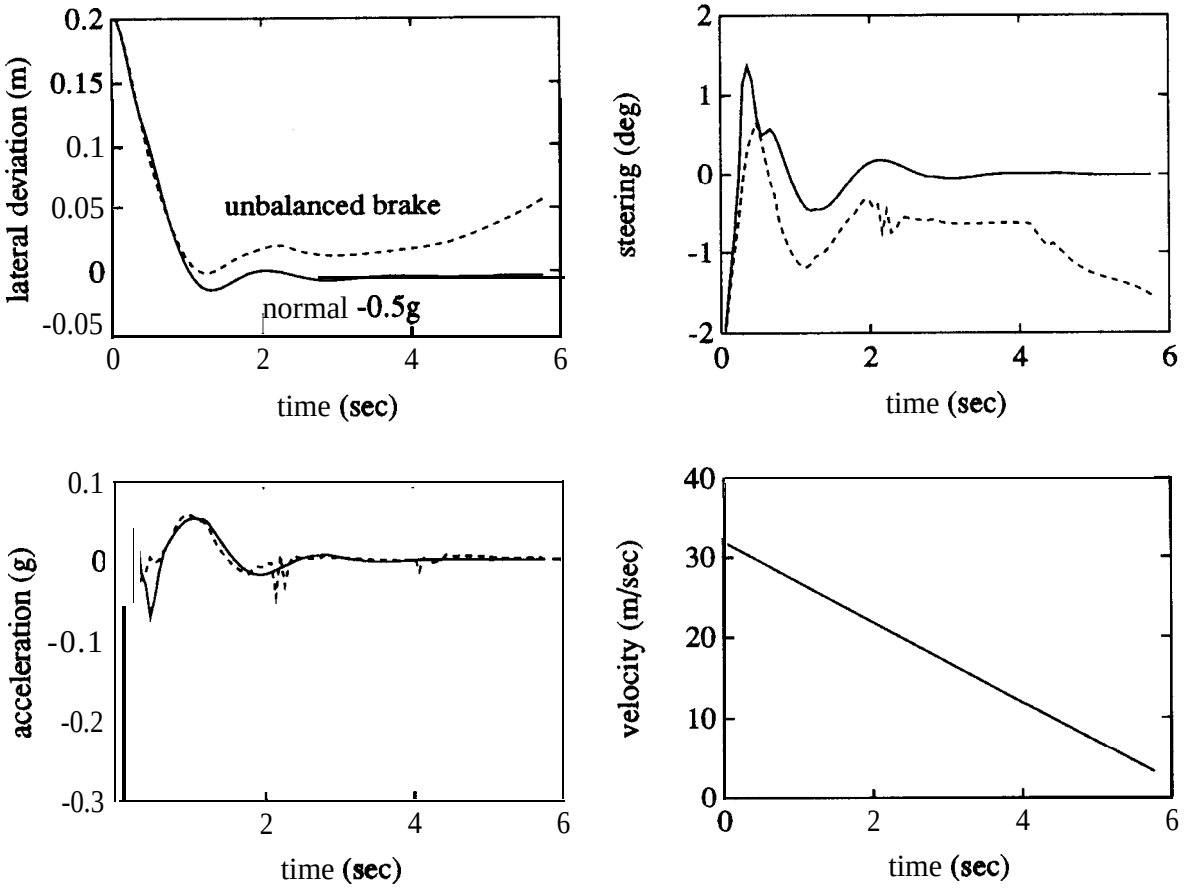

Figure 16 Simulation result of braking

those from the rear wheels. It should be noted that no braking model has been utilized, the torque needed to achieve the deceleration is assumed to be available and applied on the wheels(controlled by, say, ABS system). Two cases are presented: the solid lines represent the responses when the brakes are well balanced; and the dotted line shows the responses when the right two wheel have 33% more braking power than their left-side counterparts, i.e., the braking system is very poor-balanced, It can be seen that the controller steers the vehicle in the right direction. Although the velocity range is defined to be within 10 m/sec and 40 m/sec, the vehicle speed is decelerated to be less than 3m/sec while the lateral deviation is kept under 5cm even with unbalanced brake.

Superelevated road

It is well known that if a road is superelevated properly, vehicles can drive through a curve with a much smaller steering angle, that is, road superelevation is a road geometry parameter as important as the curvature. Figure 17 shows the vehicle responses when the road has a 6^o sinusoidal superelevation angle. The vehicle speed is 32 m/sec. Because the superelevation information is not included in the feedforward control signal, the steering angle tracks the road superelevation angle with a time delay, therefore, the lateral deviation can be as large as 4cm. This suggests that if tight tracking is desired, the road superelevation information should also be included in the feedforward control signal.

6 Conclusions

The FSLQ feedback control theory has been utilized to include the “ride quality” in the performance index explicitly in the design of the lateral feedback controller. Furthermore, by properly choosing the weighting factors in the performance index, the high frequency robustness of the controller can be enhanced. The FSLQ problem was transformed to a standard LQ problem by introducing augmented state variables, and the optimal control gains were computed by solving a Riccati equation. A feedforward controller is used to generate the steady-state steering command when the vehicle is in a curved section.

An estimator for the cornering stiffness C_s has been developed. This identification algorithm required two sensors: a lateral accelerometer and a yaw rate sensor. Simulation results showed that this algorithm estimates the true value of the cornering stiffness with an error less than 7%.

Numerical simulation results show that this control system has good disturbance rejection capability, and the discrete marker scheme does not cause a

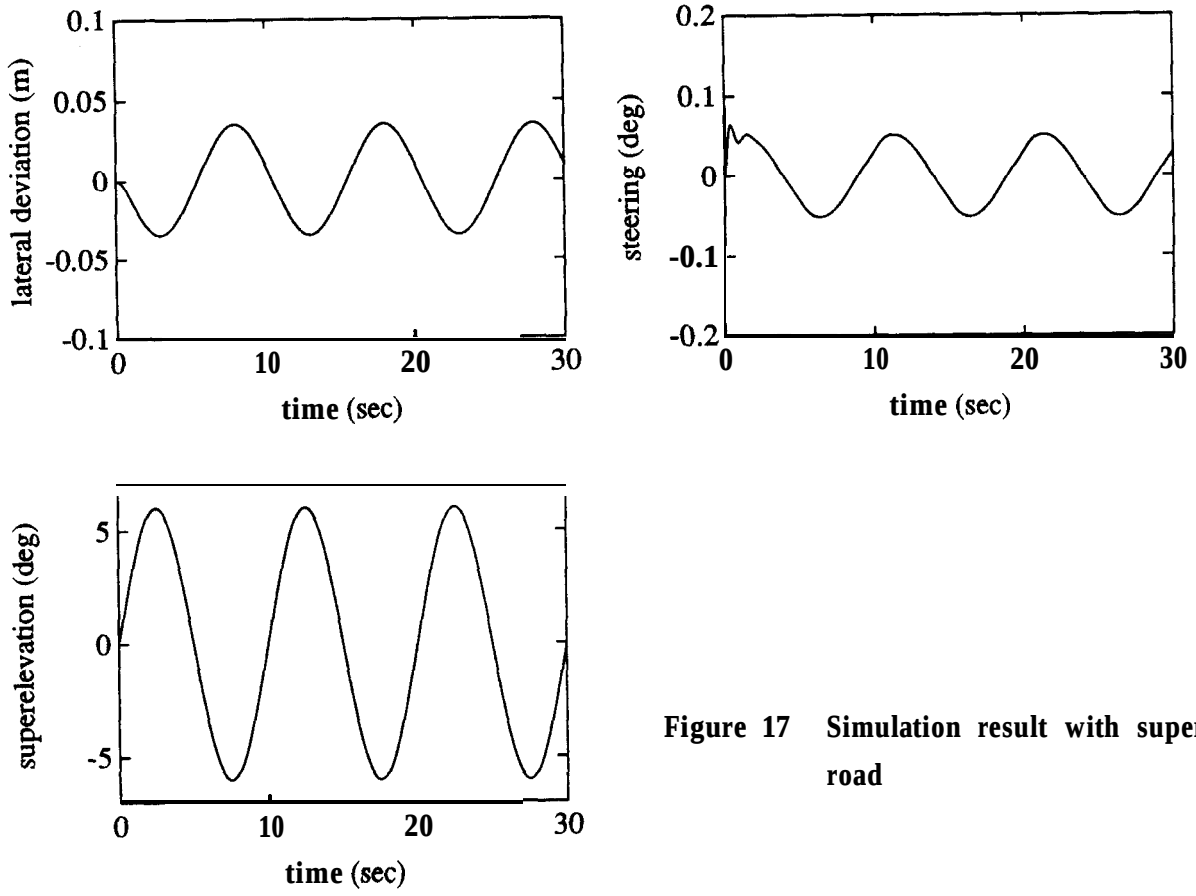

Figure 17 **Simulation result with superelevated road**

significant degradation of performance. When a section of icy road is present, the FSLQ controller with fixed gains fails to keep the tracking error to be less than 20 cm. Yet, when the gain scheduling technique is applied, the controller performs satisfactorily. Moreover, it has been shown that the performance of the controller is acceptable even under an emergency braking condition.

Appendix 1

Figure Al .l indicates the scope of the vehicle complex model. The dynamics of this model are described by sixteen state variables, two in each of the longitudinal, lateral, vertical, roll, pitch, and yaw directions and four for the tires. The inputs are the steering angles and traction (or braking) torques acting on the four tires. These inputs can be independently specified in the model. Therefore, this model is suited for four-wheel-steering, four-wheel-drive vehicles. However, at this stage of the PATH project, we use this model only for a front-wheel-steering, front-wheel-drive vehicle.

The dynamic equations are derived based on the results of Lugner[131, with some changes in state variables and tire models. In this model, the roll and pitch motions of the mass center are assumed to be relative to their undisturbed positions. The yaw motion relative to the chassis is assumed to be small, therefore, the yaw angle used is with respect to an inertial coordinate. The nomenclatures of the complex model are summarized below:

x :	motion in longitudinal direction
y :	motion in lateral direction
z :	motion in vertical direction
ϕ :	roll angle
θ :	pitch angle
ε :	yaw angle
β :	vehicle side slip angle
ψ :	vehicle velocity angle $\psi = \varepsilon + \beta$
γ :	super-elevation angle
δ_i :	steering angle of *i*th tire
F_{xi} :	traction(braking) force on ith tire
F_{yi} :	side force on ith tire
F_{Ai} (F_{Bi}) :	longitudinal(lateral) force from *ith* tire
P_i :	normal force from ith tire
$M_X(M_Y)(M_Z)$:	moment in x (y)(z) direction
I_x $(I_y)(I_z)$:	moment of inertia in x (y)(z) direction
F_{wx} (F_{wy}) :	wind force in x (y) direction
l_1 (l_2) :	distance from c.g. to front (rear) axle

--

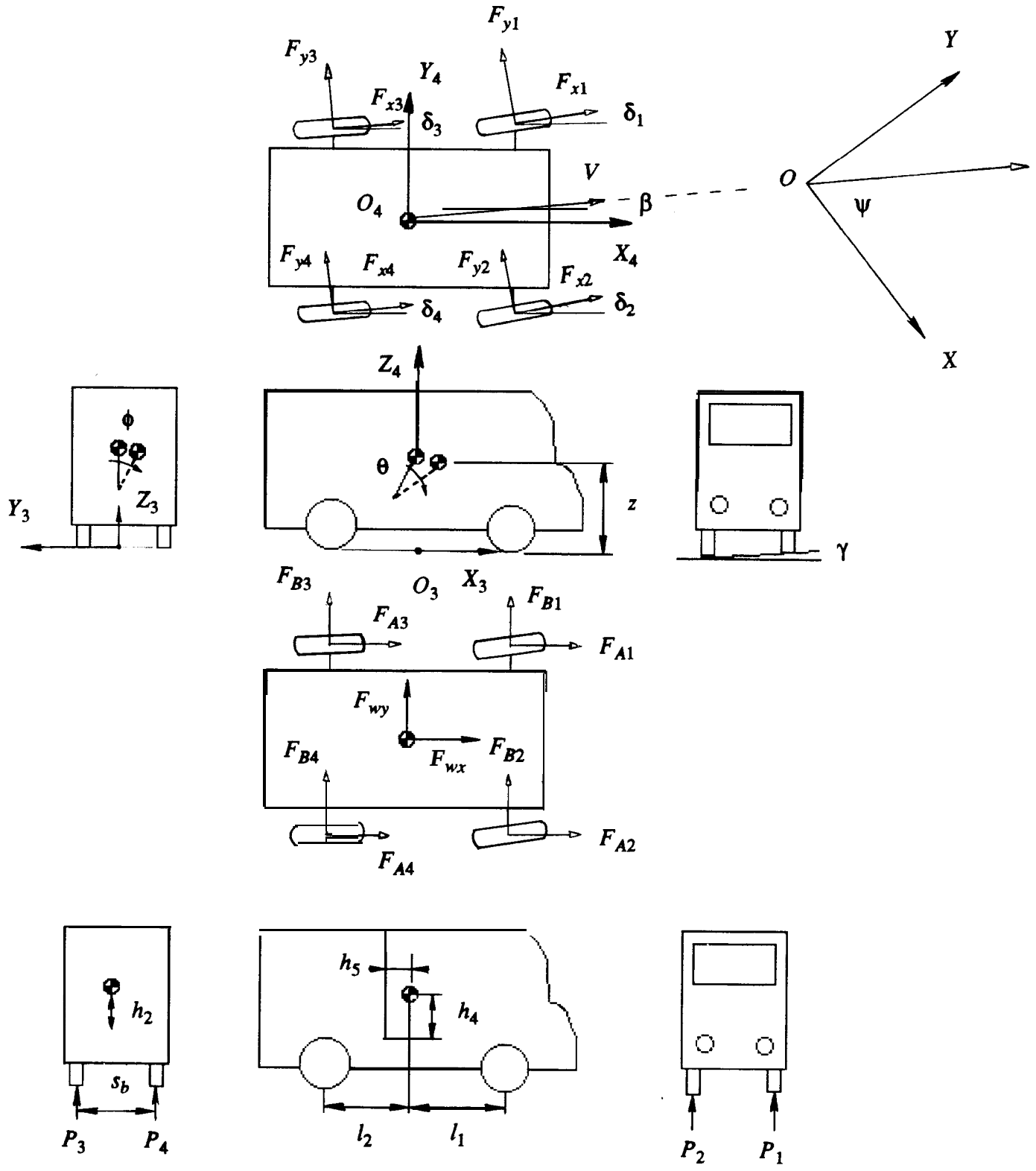

Figure Al.1 Schematic diagram of the complex vehicle model

h_2 :	distance from c.g. to roll center
h_4 (h_5) :	z(x)-distance from c.g. to pitch center
s_b :	track

In the derivation of the dynamic equations, the angles $\phi, \theta, \beta, \gamma$, and δ_i are assumed to be small, so that $\sin(\theta) \simeq 8$, $\cos(\theta) \simeq 1$, etc. Referring to Figure A1.1, let V_{o3} represent the velocity of the point O_3, the projection point of the mass center (O_4) on the road surface with respect to the $O_3X_3Y_3Z_3$ coordinate, and ω_{o3} be the angular velocity of the point O_3 with respect to the $O_3X_3Y_3Z_3$ coordinate, we have:

$$V_{o3} = (\dot{x}, \dot{y}, 0)^T \tag{A11}$$

$$\dot{V}_{o3} = \frac{d}{dt}(V_{o3}) + \omega_{o_3} \times V_{o3} \tag{Al .2}$$

It can be seen from Figure Al.1 that

$$\omega_{o3} = (\dot{\gamma}, \dot{\gamma}\beta - \dot{\psi}\gamma, \dot{\psi} - \dot{\beta})^T \tag{A1.3}$$

$$\omega_{o4/o3} = (\dot{\phi}, \dot{\theta}, 0)^T \tag{Al .4}$$

From (A1.3) and (A1.4),

$$\omega_{o4} = (\dot{\phi} + \dot{\gamma}, \dot{\gamma}\beta - \dot{\psi}\gamma + \dot{\theta}, \dot{\psi} - \dot{\beta})^T \tag{Al .5}$$

$$\dot{\omega}_{o4} = (\ddot{\phi} + \ddot{\gamma}, \ddot{\gamma}\beta + \dot{\gamma}\dot{\beta} - \ddot{\psi}\gamma - \dot{\psi}\dot{\gamma} + \ddot{\theta}, \ddot{\psi} - \ddot{\beta})^T$$

Substituting (Al. 1) and (A1.3) to (Al .2), we obtain

$$\dot{V}_{o3} = [\ \ddot{x} - \dot{y}\dot{\varepsilon}, \ddot{y} + \dot{x}\dot{\varepsilon}, \ \dot{\gamma}\dot{y} - \dot{x}(\dot{\gamma}\beta - \dot{\psi}\gamma)\ ]^T \tag{Al .6}$$

Note that the quantities ω_{o4} and $\omega_{o4/4}$ in (A1.5) are measured in the $O_3X_3Y_3Z_3$ coordinate. Let $\omega_{o4/4}$ represent the angular velocity of the mass center with respect to the coordinate $O_4X_4Y_4Z_4$ which is fixed on the car body (sprung mass). Assuming that θ, ϕ are small, we have

$$\omega_{o4/4} = \begin{bmatrix} 1 & 0 & -\theta \\ 0 & 1 & \phi \\ \theta & -\phi & 1 \end{bmatrix} \begin{bmatrix} \dot{\phi}+\dot{\gamma} \\ \dot{\gamma}\beta - \dot{\psi}\gamma + \dot{\theta} \\ \dot{\psi} - \dot{\beta} \end{bmatrix} = \begin{bmatrix} \dot{\phi} + \dot{\gamma} - \theta(\dot{\psi} - \dot{\beta}) \\ \dot{\gamma}\beta - \dot{\psi}\gamma + \dot{\theta} + \phi(\dot{\psi} - \dot{\beta}) \\ \dot{\psi} - \dot{\beta} + \theta(\dot{\phi} + \dot{\gamma}) - \phi(\dot{\gamma}\beta - \dot{\psi}\gamma + \dot{\theta}) \end{bmatrix} \tag{A1.7}$$

$$\dot{\omega}_{o4/4} \simeq \begin{bmatrix} \ddot{\phi} + \ddot{\gamma} - \dot{\theta}\dot{\varepsilon} - \theta\ddot{\varepsilon} \\ \dot{\gamma}\dot{\beta} + \ddot{\gamma}\beta - \dot{\psi}\dot{\gamma} - \ddot{\psi}\gamma + \ddot{\theta} + \phi\ddot{\varepsilon} + \dot{\phi}\dot{\varepsilon} \\ \ddot{\varepsilon} + \dot{\theta}\dot{\gamma} + \theta(\ddot{\phi} + \ddot{\gamma}) - \phi\ddot{\theta} \end{bmatrix} \tag{A1.8}$$

The distance from O_4 to O_3 varies when the vehicle is subject to roll, pitch and vertical motions, in $O_3X_3Y_3Z_3$ coordinate it can be expressed as:

$$r_{o4/o3} = (h_4\theta, -h_2\phi, z - h_5\theta)^T \quad \text{(Al .9)}$$

The relative velocity and acceleration between O_4 and O_3 can be obtained by differentiating (Al .9):

$$\dot{r}_{o4/o3} = \frac{d}{dt} r_{o4/o3} + \omega_{o3} \times r_{o4/o3}$$

$$\approx [h_4\dot{\theta}+z(\dot{\gamma}\beta-\dot{\psi}\gamma)+h_2\phi\dot{\varepsilon}, -h_2\dot{\phi} + h_4\theta\dot{\varepsilon}-\dot{\gamma}(z - h_5\theta), \dot{z}-h_5\dot{\theta} - h_2\phi\dot{\gamma}]^T \quad \text{(A1.lO)}$$

$$\ddot{r}_{o4/o3} \approx [\, h_4\ddot{\theta}, -h_2\ddot{\phi} - z\ddot{\gamma}, \ddot{z} - h_5\ddot{\theta}\,]^T \quad \text{(A1.ll)}$$

From (A1.6) and (A1.11),

$$\ddot{r}_{o4} = \ddot{r}_{o4/o3} + \dot{V}_{o3} \approx \begin{bmatrix} \ddot{x} - \dot{y}\,\dot{\varepsilon} + h_4\ddot{\theta} \\ \ddot{y} + \dot{x}\,\dot{\varepsilon} - h_2\ddot{\phi} - z\ddot{\gamma} \\ \dot{\gamma}\,\dot{y} - \dot{x}\,(\dot{\gamma}\,\beta - \dot{\psi}\,\gamma) + \ddot{z} - h_5\ddot{\theta} \end{bmatrix} \quad \text{(A1.12)}$$

Equation (Al .12) gives the accelerations of the mass center in the three translational directions when the vehicle is subject to external forces. The dynamic equations governing the angular motions of the vehicle are obtained from the Euler equations:

$$\sum M_x = I_x\,\dot{\omega}_x - (I_y - I_z)\omega_y\,\omega_z \quad \text{(A1.13)}$$

$$\sum M_y = I_y\,\dot{\omega}_y - (I_z - I_x)\omega_z\,\omega_x \quad \text{(A1.14)}$$

$$\sum M_z = I_z\,\dot{\omega}_z - (I_x - I_y)\omega_x\,\omega_y \quad \text{(A1.15)}$$

where I,, I_y and I_z are the moments of inertia of the car body along its principal axes. Assuming that the principal axes coincide with the $X_4Y_4Z_4$ axes(Figure A1.1), the components of ω and $\dot{\omega}$ are those shown in Equations (A1.7) and (Al .8) respectively.

External inputs in this model include wind forces, tire forces, and the corresponding moments generated from the tire forces. They are modeled as follows:

Wind forces:

$$F_{wx} = -K_x\dot{x}^2 \quad \text{(A1.16)}$$

$$F_{wy} = -K_y\dot{y}^2 \quad \text{(A1.17)}$$

where F_{wx} and F_{wy} are the wind forces in x and y directions, and K_x and K_y are the corresponding wind resistance coefficients. The quadratic relation between velocity and drag force is assumed.

Tire forces:

$$F_{Ai} = F_{xi}\cos(\delta_i) - F_{yi}\sin(\delta_i) \qquad i=1..4 \qquad \text{(A1.18)}$$

$$F_{Bi} = F_{xi}\sin(\delta_i) + F_{yi}\cos(\delta_i) \qquad i=1..4 \qquad \text{(A1.19)}$$

$$P_i = \frac{mgl_2}{2(l_1+l_2)} + P_{Di} + P_{Fi} \qquad i=1,2 \qquad \text{(Al .20)}$$

$$P_i = \frac{mgl_1}{2(l_1+l_2)} + P_{Di} + P_{Fi} \qquad i=3,4 \qquad \text{(Al .21)}$$

The four tires are numbered as labeled in Fig. Al .1. F_{xi} and F_{yi} are the longitudinal and lateral forces along the tire orientation. The first, second, and third term in (A1.20) (and (A1.21)) are contributed by gravity, shock absorber and spring of suspension system respectively.

The forces F_{xi} and F_{yi} are computed from the tire model [14]. P_{Di} and P_{Fi} are computed from the suspension model [13]. These two models are described below.

Tire model:

When the characteristics of the tire (tire pressure, road and tire surface condition, temperature, etc) are fixed, the traction and turning forces generated from the tire are solely determined by the tire slip angle a and tire slip ratio s.

The tire slip angle is the angle between the tire orientation and its forward velocity. That is,

$$\alpha_i = \delta_i - \zeta_i \qquad \text{(Al .22)}$$

where δ_i is the ground steering angle and ζ_i is the orientation angle of velocity of the ith tire. δ_i's are set by the steering controller and ζ_i's are computed from:

$$\tan(\zeta_1) = \frac{\dot{y} + l_1\dot{\varepsilon}}{\dot{x} - \frac{s_b\dot{\varepsilon}}{2}} \qquad \tan(\zeta_2) = \frac{\dot{y} + l_1\dot{\varepsilon}}{X + \frac{s_b\dot{\varepsilon}}{2}} \qquad \text{(Al .23)}$$

$$\tan(\zeta_3) = \frac{\dot{y} - l_2\dot{\varepsilon}}{\dot{x} - \frac{s_b\dot{\varepsilon}}{2}} \qquad \tan(\zeta_4) = \frac{\dot{y} - l_2\dot{\varepsilon}}{\dot{x} + \frac{s_b\dot{\varepsilon}}{2}}$$

The tire slip ratio is defined by:

$$\textbf{During braking}\quad s_i = \frac{V_i \cos(\alpha_i) - r_i\omega_i}{V_i \cos(\alpha_i)} \qquad \text{(Al .24)}$$

$$\textbf{During traction}\quad s_i = \frac{V_i \cos(\alpha_i) - r_i\omega_i}{r_i\omega_i} \qquad \text{(Al .25)}$$

where V_i is the translational speed of the center of the tire computed from:

$$V_1 = [(\dot{y} + l_1\dot{\varepsilon})^2 + (\dot{x} - \frac{s_b\varepsilon}{2})^2]^{0.5} \qquad \text{(Al .26)}$$

$$V_2 = [(\dot{y} + l_1\dot{\varepsilon})^2 + (\dot{x} + \frac{s_b\varepsilon}{2})^2]^{0.5} \qquad \text{(Al .27)}$$

$$V_3 = [(\dot{y} - l_2\dot{\varepsilon})^2 + (\dot{x} - \frac{s_b\varepsilon}{2})^2]^{0.5} \qquad \text{(Al .28)}$$

$$V_4 = [(\dot{y} - l_2\dot{\varepsilon})^2 + (\dot{x} + \frac{s_b\varepsilon}{2})^2]^{0.5} \qquad \text{(Al .29)}$$

r_i in (A1.24) and (A1.25) is the effective rolling radius, and ω_i is the angular velocity of the *ith* tire. r_i is computed by:

$$r_i = r_{io} - \frac{P_i}{K_{iz}} \qquad \text{(Al .30)}$$

where r_{io} is the original radius of the ***ith*** tire, P_i is the vertical load, and K_{iz} is the spring constant of the ***ith*** tire in the vertical direction.

To describe the tire force model, additional parameters need to be introduced. In order to simplify the presentation, the subscript ***i*** is omitted in the sequel. The parameters which determine the road-tire interactions are:

RC :	characteristic coefficient of road-tire interaction
$C = C_o$*RC :*	stiffness constant of tire-road interface
$\nu_s = \nu_{s_o}$*RC :*	static friction coefficient
$\nu_d = \nu_{d_o}$*RC :*	sliding friction coefficient
l_t :	contact length of tire with ground
w_t :	width of tire
P :	normal load on the tire

The contact length of tire with ground is given by:

$$l_t = 2\,(\,r_o^2 - r\text{-}2\,)^{0.5} \qquad \text{(A1.31)}$$

Three intermediate parameters are defined to simplify the final expression:

$$k_t = \frac{c\ w_t\ l_t^2}{2} \qquad \text{(Al .32)}$$

$$h_t = [\ (\tan(\alpha))^2 + s^2\ ]^{-0.5} \qquad \text{(Al .33)}$$

$$q_t = \frac{k_t}{3\ \nu_s\ P\ h_t} \qquad \text{(Al .34)}$$

The longitudinal and lateral forces F_x and F_y can be expressed as follows:

During braking

$$F_x = k_t\ s\ (1 - q_t)^2 \cos(\alpha) + P\ \nu_d\ q_t^2\ (3 - 2q_t) h_t\ s - f_r\ P \qquad \text{(Al .35)}$$

$$F_y = k_t\ (1 - s)(1 - q_t)^2 \sin(\alpha) + P\ \nu_d\ q_t^2\ h_t(3 - 2q_t) \tan(\alpha) \qquad \text{(Al .36)}$$

During traction

$$F_x = k_t\ s\ (1 - q_t)^2 + P\ \nu_d\ q_t^2\ (3 - 2q_t) h_t\ s - f_r\ P \qquad \text{(Al .37)}$$

$$F_y = k_t\ (1 - s)(1 + s)(1 - q_t)^2 \tan(\alpha) + P\ \nu_d\ q_t^2\ h_t(3 - 2q_t) \tan(\alpha) \qquad \text{(A1.38)}$$

where f_r is the rolling resistance coefficient of the tire. The characteristics of the tire are shown in Fig A1.2.

Suspension model

The suspension of the vehicle is assumed to be composed of a spring and a shock absorber. The spring and damping forces are functions of the deflections at the suspension joints from their equilibrium positions. These deflections are calculated from:

$$e_1 = z_0 - z + h_5\theta + l_1\theta - \frac{s_b}{2}\phi \qquad \text{(Al .39)}$$

$$e_2 = z_0 - z + h_5\theta + l_1\theta + \frac{s_b}{2}\phi \qquad \text{(Al .40)}$$

$$e_3 = z_0 - z + h_5\theta - l_2\theta - \frac{s_b}{2}\phi \qquad \text{(Al .41)}$$

$$e_4 = z_0 - z + h_5\theta - l_2\theta + \frac{s_b}{2}\phi \qquad \text{(Al .42)}$$

where z is the original height of the mass center relative to the ground.

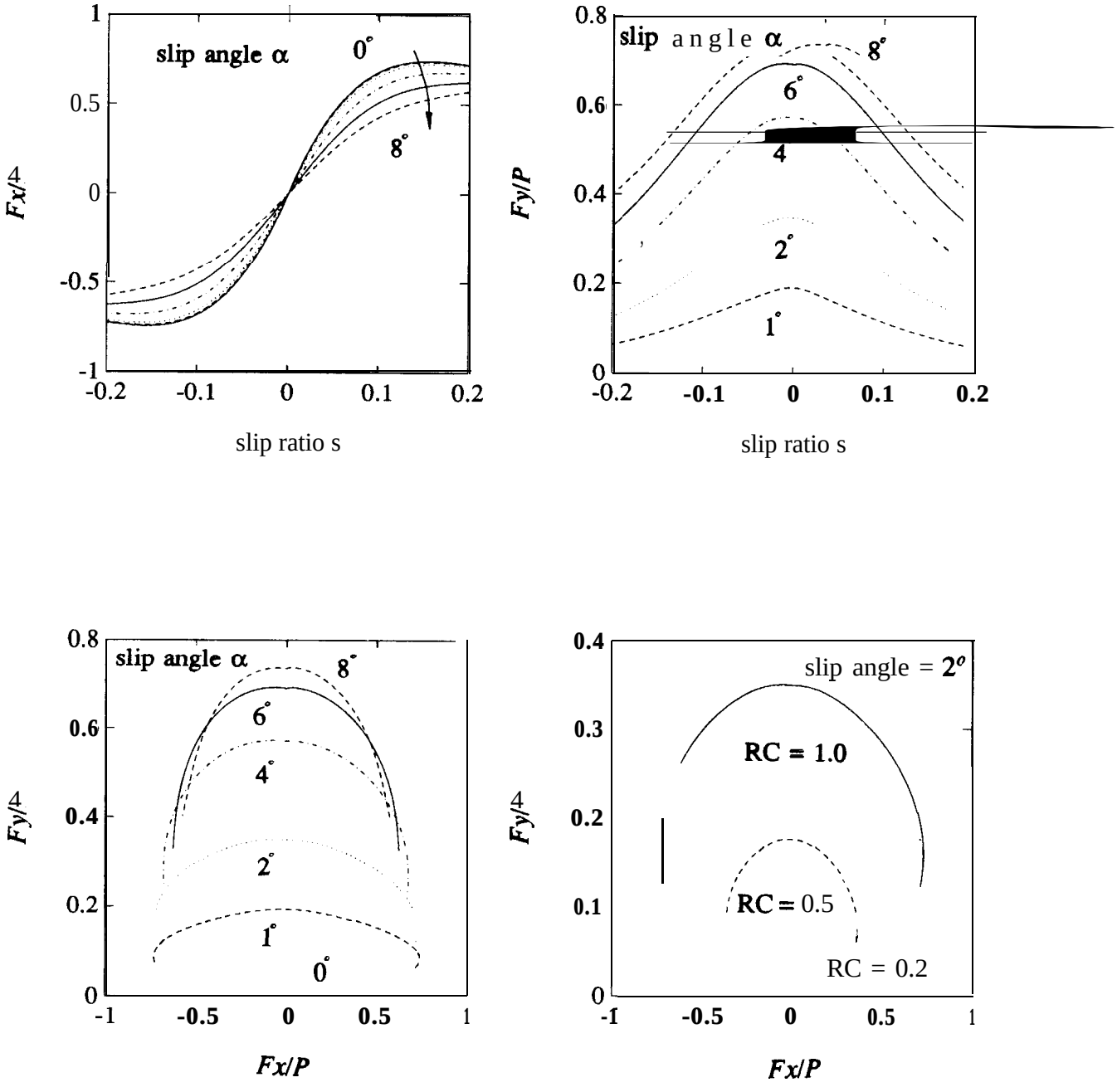

Figure Al.2 Characteristics of tire model

The spring force is given by:

$$P_{Fi} = C_{1i}(e_i + C_{2i}\, e_i^5) \qquad i = 1..4 \qquad \text{(Al .43)}$$

where C_{1i}, C_{2i} are the spring constants. If $C_{2i} > 0$, (A1.43) describes a hardening spring.

The damping force is modeled as:

$$\begin{aligned} P_{Di} &= D_i\, \dot{e}_i && |\dot{e}_i| < \bar{w} \quad \text{i} = 1..4 \\ &= D_i\, \bar{w} + \bar{D}_i\, (\dot{e}_i - \bar{w}) && \dot{e}_i \geq \bar{w} \\ &= -D_i\, \bar{w} + \bar{D}_i\, (\dot{e}_i + \bar{w}) && \dot{e}_i \leq -\bar{w} \end{aligned} \qquad \text{(Al 44)}$$

That is, the hysteresis effect is neglected, and the force-velocity characteristic of the damper is approximated by three straight lines.

Moments:

Using (Al .18)-(A1.21), the moments acting on the vehicle through the tires can be computed as:

$$M_{X3} = (\frac{s_b}{2} + h_2\phi)(P_1 + P_3) - (\frac{s_b}{2} - h_2\phi)(P_2 + P_4) + (z - h_5\theta)\sum_{i=1}^{4} F_{Bi} \qquad \text{(A1.45)}$$

$$M_{Y3} = (l_2 + h_4\theta)(P_3 + P_4) - (l_1 - h_4\theta)(P_1 + P_2) - (z - h_5\theta)\sum_{i=1}^{4} F_{Ai} \qquad \text{(Al .46)}$$

$$\begin{aligned} M_{Z3} = {} & (l_1 - h_4\theta)(F_{B1} + F_{B2}) - (l_2 + h_4\theta)(F_{B3} + F_{B4}) \\ & - (\frac{s_b}{2} + h_2\phi)(F_{A1} + F_{A3}) + (\frac{s_b}{2} - h_2\phi)(F_{A2} + F_{A4}) \end{aligned} \qquad \text{(Al .47)}$$

where M_{X3}, M_{Y3} and M_{Z3} are the moments in the X_3, Y_3 and Z_3 directions respectively. Remember that the sprung mass rotate relative to the unsprung mass with roll and pitch motions. To use the Euler's equations (A1.13)-(A1.15), the moments must be expressed in the principal axes X_4, Y_4 and Z_4. They are given as:

$$\begin{bmatrix} M_{X4} \\ M_{Y4} \\ M_{Z4} \end{bmatrix} = \begin{bmatrix} 1 & 0 & -\theta \\ 0 & 1 & \phi \\ \theta & -\phi & 1 \end{bmatrix} \begin{bmatrix} M_{X3} \\ M_{Y3} \\ M_{Z3} \end{bmatrix} \qquad \text{(Al .48)}$$

The angular velocity of the vehicle expressed in the $O_4X_4Y_4Z_4$ coordinates is shown in (A1.7). Substituting (A1.7), (Al.8) and (A1.48) to (A1.13)-(A1.15), and combining (Al .18)-(A.21) with (Al .12), the dynamic equations of the vehicle are then obtained as follows:

$$m(\ddot{x} - \dot{y}\,\dot{\varepsilon} + h_4\ddot{\theta}) = F_{wx} - mgy\,\beta + \sum_{i=1}^{4} F_{Ai} \qquad \text{(Al .49)}$$

$$m(\ddot{y} + \dot{x}\dot{\varepsilon} - h_2\ddot{\phi} - z\ddot{\gamma}) = F_{wy} - mgy + \sum_{i=1}^{4} F_{Bi} \quad \text{(Al SO)}$$

$$m(\ddot{z} - h_5\ddot{\theta} - \dot{x}(\dot{\gamma}\beta - \dot{\psi}\gamma) + \dot{\gamma}\dot{y}) = -mg + \sum_{i=1}^{4} P_i \quad \text{(A1.51)}$$

$$I_x(\ddot{\gamma} + \ddot{\phi} - \theta\ddot{\varepsilon}) - (I_y - I_z + I_x)\,\dot{\theta}\dot{\varepsilon} = M_{X3} - \theta M_{Z3} \quad \text{(A1.52)}$$

$$I_y(\ddot{\theta} + \ddot{\gamma}\beta + \phi\ddot{\varepsilon} - \gamma\ddot{\psi}) + (I_x - I_y - I_z)\,\dot{\gamma}\dot{\varepsilon} + (I_x + I_y - I_z)\dot{\phi}\dot{\varepsilon} = M_{Y3} + \phi M_{Z3} \quad \text{(A1.53)}$$

$$I_z[\ddot{\varepsilon} + \theta(\ddot{\gamma} + \ddot{\phi}) - \phi\ddot{\theta}] - (I_x - I_y - I_z)\,(\dot{\gamma} + \dot{\phi})\,\dot{\theta} - I_z\,\dot{\phi}\,\dot{\theta} = M_{Z3} + \theta M_{X3} - \phi M_{Y3} \quad \text{(A1.54)}$$

The values of the parameters used in the simulations are listed in Table A.1 for reference.

Table A.1 System parameters of the complex model

parameter	unit	value	parameter	unit	value
C_0	kg/m^3	9.843E5	C_{1i}	N/m	40000
C_{2i}	$1/m^4$	40000	D_i	$(N\text{–sec})/m$	10000
$\overline{D_i}$	$(N\text{–sec})/m$	4000	f_r	-	0.02
h_2	m	0.43	h_4	m	0.4
h_5	m	0.1	I_x	$Kg\text{–}m^2$	460
I_y	$Kg\text{–}m^2$	2300	I_z	$Kg\text{–}m^2$	3100
K_{iz}	Kg/m	20000	K_x	$(N\text{–sec}^2)/m^2$	0.45
K_y	$(N\text{–sec}^2)/m^2$	2.1	l_1	m	1.15
l_2	m	1.51	m	Kg	1550
r_0	m	0.3	s_b	m	1.5
w_t	m	0.2	$\overline{w}$	m/sec	0.025
z_0	m	0.6	ν_{s_0}	-	1.0
ν_{d_0}	-	0.7	τ	msec	32

Appendix 2

The simplified model is derived from the complex model. Assuming that the vertical, roll, and pitch motions can be neglected, the superelevation of road, side slip angle, and error in yaw angle $(\varepsilon - \varepsilon_d)$ are small, and the longitudinal velocity is constant, the complex model derived in Appendix 1 can be simplified to a linear model. The number of state variables is only four, two for each of the lateral and yaw motions. Referring to Figure A2.1, nomenclatures for the simplified model are as follows :

y_r : lateral distance between the mass center and the center line of road

ε : yaw angle of vehicle body

ε_d : desired yaw angle set by the road

d_s : distance from vehicle mass center to magnetic sensor

V : longitudinal velocity of vehicle

ρ : radius of curvature of the road

6 : front wheel steering angle

Other variables not explicitly stated here are similarly defined as the complex model. Assuming that y,., $\varepsilon - \varepsilon_d$, and $\dot{\varepsilon}$ are small, the following equations can be obtained from (A1.50) and (A1.54):

$$\ddot{y} + V\dot{\varepsilon} \approx \ddot{y}_r + \frac{V^2}{\rho} \tag{A2.1}$$

$$m(\ddot{y}_r + \frac{V^2}{\rho}) = F_{wy} + \sum_{i=1}^{4} F_{Bi} \tag{A2.2}$$

$$I_z \ddot{\varepsilon} = M_{Z3} \tag{A2.3}$$

The original definition of the cornering stiffness C_s is as follows [14]:

$$C_s = \frac{\partial F_y}{\partial \alpha}\Big|_{\alpha = 0} \tag{A2.4}$$

The C_s is assumed to be constant in the simplified model, that is, the lateral force generated from the tire is assumed to be proportional to the tire slip angle:

$$F_y = C_s \, a \tag{A2.5}$$

The rate of the lateral deviation between the mass center and the center of road is:

$$\dot{y}_r = \dot{y} + V (\varepsilon - \varepsilon_d) \tag{A2.6}$$

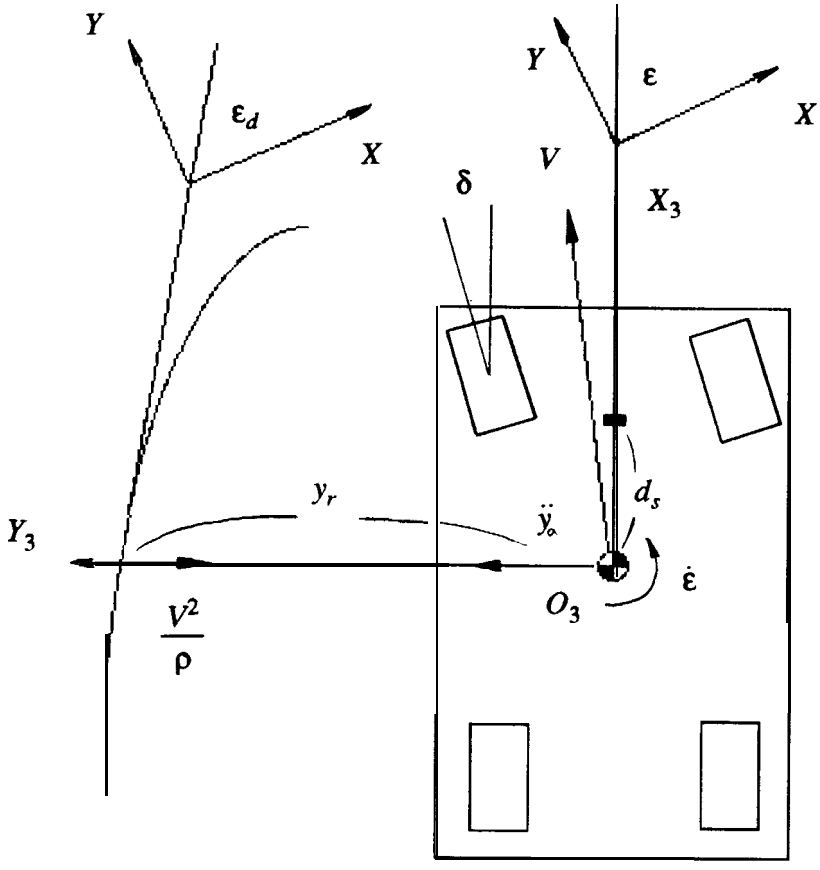

Figure A2.1 Schematic diagram of the simplified vehicle model

Assuming that $\dot{x} >> s\dot{\varepsilon}$, we obtain from (A2.6) and (A1.23):

$$F_{yi} = C_{si}\left(\delta_i - \frac{\dot{y}_r + l_1\dot{\varepsilon}}{V} + \varepsilon - \varepsilon_d\right) \qquad i=1,\ 2 \qquad \text{(A2.7)}$$

$$F_{yi} = C_{si}\left(\delta_i - \frac{\dot{y}_r - l_2\dot{\varepsilon}}{V} + \varepsilon - \varepsilon_d\right) \qquad i=3,4 \qquad \text{(A2.8)}$$

Assuming that the angles are small in (Al .18), (Al .19) and (Al .47), we obtain:

$$\sum_{i=1}^{4} F_{Bi} = \sum_{i=1}^{4} F_{yi} + \sum_{i=1}^{4} F_{xi}\,\delta_i \qquad \text{(A2.9)}$$

$$M_{Z3} = l_1(F_{B1} + F_{B2}) - l_2(F_{B3} + F_{B4}) - \frac{s_b}{2}(F_{A1} + F_{A3}) + \frac{s_b}{2}(F_{A2} + F_{A4}) \qquad \text{(A2.10)}$$

Since we are considering front-wheel-steer, front-wheel-drive vehicles, let $\delta_1 = \delta_2 = 6$, $\delta_3 = \delta_4 = 0$ and $F_{x3} = F_{x4} = 0$. By substituting (A2.9) to (A2.2) and (A2.10) to (A2.3),

$$\ddot{y}_r = \frac{A_1}{V}\dot{y}_r - A_1(\varepsilon - \varepsilon_d) + \frac{A_2}{V}(\dot{\varepsilon} - \dot{\varepsilon}_d) + B_1\delta + d_1 \qquad \text{(AZ.1 1)}$$

$$\ddot{\varepsilon} - \ddot{\varepsilon}_d = \frac{A_3}{V}\dot{y}_r - A,(\varepsilon - \varepsilon_d) + \frac{A_4}{V}(\dot{\varepsilon} - \dot{\varepsilon}_d) + B_2\delta + d_2 \qquad \text{(AZ. 12)}$$

where

$$A, = \frac{-1}{m}[C_{s1} + C_{s2} + C_{s3} + C_{s4}] \qquad \text{(A2.13)}$$

$$A_2 = \frac{1}{m}[-l_1(C_{s1} + C_{s2}) + l_2(C_{s3} + C_{s4})\ 1 \qquad \text{(AZ. 14)}$$

$$A_3 = \frac{1}{I_z}[-l_1(C_{s1} + C_{s2}) + l_2(C_{s3} + C_{s4})\ 1 \qquad \text{(A2.15)}$$

$$A_4 = -\frac{1}{I_z}[l_1^2(C_{s1} + C_{s2}) + l_2^2(C_{s3} + C_{s4})] \qquad \text{(A2.16)}$$

$$B_1 = \frac{1}{m}[F_{x1} + F_{x2} + C_{s1} + C_{s2}] \qquad \text{(A2.17)}$$

$$B_2 = \frac{l_1}{I_z}[F_{x1} + F_{x2} + C_{s1} + C_{s2}] \qquad \text{(A2.18)}$$

$$d_1 = \frac{F_{wy} + F_{disturb}}{m} - \frac{V^2}{\rho} + \frac{A_2}{V}\dot{\varepsilon}_d = \bar{d}_1 - V\dot{\varepsilon}_d + \frac{A_2}{V}\dot{\varepsilon}_d \qquad \text{(A2.19)}$$

$$d_2 = \frac{T_{disturb}}{I_z} + \frac{A_4}{V}\dot{\varepsilon}_d - \ddot{\varepsilon}_d = \bar{d}_2 + \frac{A_4}{V}\dot{\varepsilon}_d - \ddot{\varepsilon}_d \qquad \text{(A2.20)}$$

In Eqs. (A2.19) and (A2.20) $F_{disturb}$ and $T_{disturb}$ are the disturbance force and torque acting on the vehicle. The simplified model (A2.11) and (A2.12) can be written in the state-space form,

$$\frac{d}{dt}\begin{vmatrix} y_r \\ \dot{y}_r \\ \varepsilon-\varepsilon_d \\ \dot{\varepsilon}-\dot{\varepsilon}_d \end{vmatrix} = \begin{vmatrix} 0 & 1 & 0 & o \\ 0 & \frac{A_1}{V} & -A, & \frac{A_2}{V} \\ 0 & 0 & 0 & 1 \\ 0 & \frac{A_3}{V} & -A_3 & \frac{A_4}{V} \end{vmatrix} \begin{bmatrix} y_r \\ \dot{y}_r \\ \varepsilon-\varepsilon_d \\ \dot{\varepsilon}-\dot{\varepsilon}_d \end{bmatrix} + \begin{bmatrix} 0 \\ B_1 \\ 0 \\ B_2 \end{bmatrix} \delta + \begin{bmatrix} 0 \\ d_1 \\ 0 \\ d_2 \end{bmatrix} = A\,\underline{x} + \underline{B}\,\delta + \underline{d} \quad \text{(A2.21)}$$

The output of the magnetometer located at a distance d_s ahead of the mass center can be expressed as :

$$y_S = y_r + d_s(\varepsilon - \varepsilon_d) = [1, 0, d_s, 0\ 1\ \underline{x} \quad \text{(A2.22)}$$

The output y_s is affected by the input signal 6, the disturbances $\bar{d}_1, \bar{d}_2$ and the reference signal (the road path). The relation can be represented in the transform domain as follows:

$$y_s(s) = \frac{1}{\Delta(s)}\left[(d_sB_2+B_1)s^2+\frac{d_s(B_1A_3-B_2A_1)+B_2A_2-B_1A_4}{V}s + B_1A_3 - B_2A_1\right]\delta(s) \quad \text{(A2.23)}$$

$$+ \frac{1}{\Delta(s)}\left[s^2 + \frac{d_sA_3-A_4}{V}\,s + A_3\right]\bar{d}_1(s) + \frac{1}{\mathrm{A(s)}}\left[d_s\,s^2 + \frac{A_2-d_sA_1}{V}\,s - A_1\right]\bar{d}_2(s)$$

$$\frac{d_s\,s + V}{s^2}\,\dot{\varepsilon}_d(s)$$

where

$$\Delta(s) = s^2\left[\,s^2 - \frac{A_1 + A_4}{V}\,s + \frac{(A_1A_4 - A_2A_3)}{V^2} + A_3\right] \quad \text{(A2.24)}$$

Appendix 3

From Appendix 2, the simplified model of the front-wheel-steering vehicle is:

$$\frac{d}{dt}\begin{vmatrix} y_r \\ \dot{y}_r \\ \varepsilon-\varepsilon_d \\ \dot{\varepsilon}-\dot{\varepsilon}_d \end{vmatrix} = \begin{vmatrix} 0 & 1 & 0 & 0 \\ 0 & \frac{A_1}{V} & -A_1 & \frac{A_2}{V} \\ 0 & 0 & 0 & 1 \\ 0 & \frac{A_3}{V} & -A_3 & \frac{A_4}{V} \end{vmatrix} \begin{bmatrix} y_r \\ \dot{y}_r \\ \varepsilon-\varepsilon_d \\ \dot{\varepsilon}-\dot{\varepsilon}_d \end{bmatrix} + \begin{vmatrix} 0 \\ B_1 \\ 0 \\ B_2 \end{vmatrix} \delta + \begin{bmatrix} 0 \\ d_1 \\ 0 \\ d_2 \end{bmatrix} = A\,\underline{x} + \underline{B}\,\delta + \underline{d} \quad \text{(A3.1)}$$

where δ is the steering angle of the front wheels, y_r is the lateral deviation of the mass center, and ε is the orientation of the vehicle in yaw direction. A_i and B_i are determined by Eqs.(A2.13)-(A2.18), and d_1 and d_2 **are** defined by (A2.19) and (A2.20). Remember that the objective of the lateral control is to keep the tracking error small and to maintain good ride quality, the performance index is chosen to be:

$$J=\frac{1}{2\pi}\int_{-\infty}^{\infty}[a^*(j\omega)\frac{q_a^2}{1+\lambda_a^2\omega^2}a(j\omega) + y_r^*(j\omega)\frac{q_y^2}{1+\lambda_y^2\omega^2}y_r(j\omega) \quad \text{(A3.2)}$$

$$+ (\varepsilon(j\omega)-\varepsilon_d(j\omega))^*\frac{q_\varepsilon^2}{1+\lambda_\varepsilon^2\omega^2}(\varepsilon(j\omega)-\varepsilon_d(j\omega)) + y_s^*(j\omega)\frac{q_i^2}{(j\omega)^2}y_s(j\omega)+\delta^*(j\omega)\delta(j\omega)]d\omega$$

where a is the difference between the total lateral acceleration $\ddot{y}_a$ and its desired value, i.e.,

$$a = \ddot{y}_a - \frac{V^2}{\rho} \approx \ddot{y}_r \quad \text{(A3.3)}$$

The first term in (A3.2) is used to represent the ride quality, the second, third and fourth terms are included for tracking capability, and the fifth term represents the control effort. The approximation $a \approx \ddot{y}_r$ is utilized in (A3.2) to change the performance index J to standard form. The FSLQ problem is transformed to a standard LQ problem by introducing augmented state variables. Let

$$z_1^* z_1 \equiv a^*(j\omega)\frac{q_a^2}{1+\lambda_a^2\omega^2}\,a(j\omega) \quad \text{(A3.4)}$$

$$z_2^* z_2 \equiv y_r^*(j\omega)\frac{q_y^2}{1+\lambda_y^2\omega^2}\, y_r(j\omega) \tag{A3.5}$$

$$z_3^* z_3 \equiv (\varepsilon(j\omega)-\varepsilon_d(j\omega))^*\frac{q_\varepsilon^2}{1+\lambda_\varepsilon^2\omega^2}\,(\varepsilon(j\omega)-\varepsilon_d(j\omega)) \tag{A3.6}$$

$$z_4^* z_4 \equiv y_s^*(j\omega)\frac{q_i^2}{(j\omega)^2}\, y_s(j\omega) \tag{A3.7}$$

Substituting the approximation (A3.3) to (A3.4), $z_1(s)$ can be expressed as:

$$z_1(s) = \frac{q_a}{1+\lambda_a s}s^2 y_r(s) \tag{A3.8}$$

Or in the time domain:

$$\dot{z}_1(t) = \frac{-1}{\lambda_a} z_1(t) + \frac{q_a}{\lambda_a}\ddot{y}_r(t) = \frac{-1}{\lambda_a} z_1(t) + \frac{q_a}{\lambda_a}[C_2\,\underline{x} + B_1\,\delta] \tag{A3.9}$$

where

$$C_2 = [\,0, \frac{A_1}{V}, -A_1, \frac{A_2}{}, I \tag{A3.10}$$

is the second row of the state matrix A in (A3.1). The disturbance d_1 is assumed to be unknown to get (A3.9).

(A3.5)-(A3.7) can be rewritten as:

$$\dot{z}_2(t) = \frac{-1}{\lambda_y} z_2(t) + \frac{q_y}{\lambda_y} y_r(t) \tag{A3.11}$$

$$\dot{z}_3(t) = \frac{-1}{\lambda_\varepsilon} z_3(t) + \frac{q_\varepsilon}{\lambda_\varepsilon}(\varepsilon(t)-\varepsilon_d(t)) \tag{A3.12}$$

$$\dot{z}_4(t) = q_i y_s(t) = q_i C\underline{x}(t) \tag{A3.13}$$

From (A3.1), (A3.9), (A3.11), (A3.12) and (A3.13), the augmented system can be put in the state space form:

$$\frac{d}{dt}\begin{vmatrix}\underline{x}\\ z_1\\ z_2\\ z_3\\ z_4\end{vmatrix} = \begin{vmatrix} A & 0 & 0 & 0 & 0 \\ \frac{q_a C_2}{\lambda_a} & \frac{-1}{\lambda_a} & 0 & 0 & 0 \\ \frac{q_y}{\lambda_Y},0,0,0] & 0 & \frac{-1}{\lambda_Y} & 0 & 0 \\ 0,0,\frac{q_\varepsilon}{\lambda_\varepsilon},0] & 0 & 0 & \frac{-1}{\lambda_\varepsilon} & 0 \\ q_i C & 0 & 0 & 0 & 0 \end{vmatrix} \begin{bmatrix}\underline{x}\\ z_1\\ z_2\\ z_3\\ z_4\end{bmatrix} + \begin{vmatrix}\underline{B}\\ \frac{q_a B_1}{\lambda_a}\\ 0\\ 0\\ 0\end{vmatrix} \delta + \begin{vmatrix}\underline{d}\\ 0\\ 0\\ 0\\ 0\end{vmatrix} \qquad \text{(A3.14)}$$

$$= A_e\, \underline{x}_e + \underline{B}_e\, \delta + \underline{d}_e$$

where $\underline{x}$ is the original fourth order state vector and $\underline{x}_e$ is the augmented state vector of eighth order.

Use the enlarged state vector in (A3.14), the performance index J of (A3.2) can be written in the standard form of a LQ problem as follows:

$$J = \frac{1}{2}\int_0^\infty [\, z_1^T z_1 + z_2^T z_2 + z_3^T z_3 + z_4^T z_4 + \delta^T \delta]\; dt \qquad \text{(A3.15)}$$

$$= \frac{1}{2}\int_0^\infty [\underline{x}^T\; z_1^T\; z_2^T\; z_3^T\; z_4^T\; \delta] \begin{bmatrix} 0 & 0 & 0 & 0 & 0 & 0 \\ 0 & 1 & 0 & 0 & 0 & 0 \\ 0 & 0 & 1 & 0 & 0 & 0 \\ 0 & 0 & 0 & 1 & 0 & 0 \\ 0 & 0 & 0 & 0 & 1 & 0 \\ 0 & 0 & 0 & 0 & 0 & 1 \end{bmatrix} \begin{bmatrix}\underline{x}\\ z_1\\ z_2\\ z_3\\ z_4\\ \delta\end{bmatrix} dt$$

Now that the system equation is in the standard LQ form, the gain vector of the feedback controller can be computed by solving the corresponding Riccati equation. In particular, we use the solution of the algebraic Riccati equation to simplify the optimal problem and make state feedback control gain vector K to be constant. Figure 9 shows how the signal flow inside the FSLQ feedback controller. G_1, G_2, G_3 and G_4 represents the dynamic filtering effect of the augmented state equations (A3.9), (A3.11), (A3.12) and (A3.13) respectively.

References

1. L. Segel,"Theoretical Prediction and Experimental Substantiation of the Responses of the Automobile to Steering Control", Proc. Auto. Div. Instn. Mech. Eng., 1956-57, No.7.
2. J. W. Senders, A. B. Kristofferson, W. H. Levison, C. W. Dietrich, J. L. Ward, "The Attentional Demand of Automobile Driving", Highway Research Record, 1967, 195, pp.15-33.
3. J. M. Carson, W. W. Wierwille, "Development of a Strategy Model of the Driver in Lane Keeping", Vehicle System Dynamics 7(1978), pp.233-253.
4. R. E. Fenton,"Automatic Vehicle Guidance and Control -- A State of the Art Survey", IEEE Transactions on Vehicular Technology, VolVT-19, No. 1, Feb. 1970, pp.153-161.
5. E. R. Hoffman,"Human Control of Road Vehicles", Vehicle System Dynamics, 1975-76, No.5 pp.105-126.
6. D. T. McRuer, R. W. Allen, D. H. Weir, R. H. Klein, "New Results in Driver Steering Control Models", Human Factors, 1977, 19(4), pp.381-397.
7. R. W. Allen, H. T. Szostak, T. J. Rosenthal,"Analysis and Computer Simulation of Driver/Vehicle Interaction", SAE paper No. 871086, 1988.
8. S. E. Shladover et al. ,"Steering Controller Design for Automated Guideway Transit Vehicles" ASME Journal of Dynamic Systems, Measurement, and Control, March 1978, Vo1.100.
9. R. L. Nisonger, D. N. Wormley,"Dyna.mic Performance of Automated Guideway Transit Vehicles with Dual-Axle Steering", IEEE Trans. on Vehicular Technology, Vol.VT-28, No. 1, Feb. 1979, pp. 88-94.
10. R. E. Fenton, G. C. Melocik, K. W. Olson, "On the Steering of Automated Vehicles: Theory and Experiment", IEEE Trans. on Automatic Control, Vol. AC-21, No.3, June 1976.
11. Y. K. Kwak, C. C. Smith, "An Active and Passive Steering Controller Study of Rubber-Tired Automated Guideway Transit Vehicles", Trans. of the ASME, J. of Dynamic Systems, Measurement, and Control, Vo1.102, Sep. 1980, pp.168-173.
12. A. Johnson, T. Assefi, J. Lai,"Automated Vehicle Guidance Using Discrete Reference Markers", IEEE trans. on VT, Vol. VT-28, No. 1, Feb. 1979, pp.95 105.
13. P. Lugner, "The Influence of the Structure of Automobile Models and Tyre Characteristics on the Theoretical Results of Steady-state and Transient Vehicle Performance" The Dynamics of Vehicles, Proceedings 5th VSD-2nd IUTAM Symposium.

14. H. Sakai,"Theoretical and Experimental Studies on the Dynamical Properties of Tyres, Part 1: Review of Theories of Rubber Friction", International Journal of Vehicle Design, Vo1.2, No. 1, 1981, pp.78110.

15. H. Sakai,"Theoretical and Experimental Studies on the Dynamical Properties of Tyres, Part 4: Investigations of the Influences of Running Conditions by Calculation and Experiment", International Journal of Vehicle Design, Vo1.3, No. 3, 1982, pp.333-375.

16. J. Y. Wong Theorv of Ground Vehicles, John Wiley & Sons, 1978.

17. N. Gupta,"Frequency-Shaped Cost Functionals: Extension of Linear-Quadratic-Gaussian Design Methods", J. of Guidance and Control, Vo1.3, No.6, Nov-Dee 1980, pp. 529-535.

18. B. D. 0. Anderson, J. B. Moore, Optimal Control -- Linear Quadratic Methods, Chapter 9, Prentice Hall, 1990.

19. Anonymous,"A Guide to the Evaluation of Human Exposure to Whole Body Vibration," ISO/DIS 263 1. International Organization for Standardization, New York, 1972.

20. Janeway, R. N.,"Vehicle Vibration Limits to Fit the Passenger," S.A.E. Journal, Vo1.56, Aug. 1948, pp.48-49.

21. Smith, C. C., McGehee, D. Y., Healey, A. J.,"The Prediction of Passenger Riding Comfort from Acceleration Data", Transactions of ASME, Journal of Dynamic Systems, Measurement, and Control. Vo1.100, March 1978, pp.34-41.

22. Anonymous, Highwav Design Manual, California Department of Transportation, fourth edition.

23. W. Zhang, T. West, R. Parsons, "An Intelligent Roadway Reference System for Vehicle Lateral Guidance/Control", Proc. 1990 ACC, San Diego.

24. Lee, A. Y., "A Preview Steering Autopilot Control Algorithm for Four-Wheel-Steering Passenger Vehicles," Advanced Automotive Technologies- 1989, pp. 83-98, ASME.

25. K. J. Astrom, B. Wittenmatk,"Computer Controlled Systems--Theory and Design", Prentice Hall, 1990.